This manuscript has been submitted for publication in Paleoceanography-Paleoclimatology. *It has not yet undergone peer review and will probably change somewhat before it is accepted. If accepted, the final version of the manuscript will be available via the "Peer-reviewed Publication DOI" link on the EarthArXiv page. Please feel free to contact the authors with feedback.*

Early Paleocene Paleoceanography and Export Productivity in the Chicxulub Crater

Christopher M. Lowery[1]*, Heather L. Jones[2], Tim Bralower[2], Ligia Perez Cruz[3], Catalina Gebhardt[4], Michael T. Whalen[5], Elise Chenot[6], Jan Smit[7], Marcie Purkey Phillips[1], Konstantin Choumiline[8], Ignacio Arenillas[9], Jose A. Arz[9], Fabien Garcia[10], Myriam Ferrand[10], Sean P.S. Gulick[1, 11], Exp. 364 Science Party[12]

[1]Institute for Geophysics, Jackson School of Geosciences, University of Texas at Austin, USA

[2]Department of Geosciences, Pennsylvania State University, University Park, USA

[3]Instituto de Geofísica, Universidad Nacional Autónoma De México, Ciudad de México, México

[4]Alfred Wegener Institute Helmholtz Centre of Polar and Marine Research, Bremerhaven, Germany

[5]Department of Geosciences, University of Alaska Fairbanks, USA

[6]Géosciences Montpellier, Université de Montpellier, France

[7]Faculty of Earth and Life Sciences (FALW), Vrije Universiteit Amsterdam, Netherlands.

[8]Department of Earth Sciences, University of California Riverside, USA

[9]Departamento de Ciencias de la Tierra and Instituto Universitario de Investigación en Ciencias Ambientales de Aragón, Universidad de Zaragoza, E-50009, Spain

[10]Biogéosciences, Université de Bourgogne Franche-Comté, France

[11]Center for Planetary Systems Habitability, Jackson School of Geosciences, University of Texas at Austin, USA

[12]See Appendix 1

*Corresponding author: Christopher Lowery (cmlowery@utexas.edu)

Key Points

- Export productivity in the Chicxulub crater was high for the first 320 kyr after the K-Pg boundary, then declined for the next 900 kyr
- The final decline in export productivity is associated with the turnover of calcareous nannoplankton disaster assemblages
- Export productivity change is not correlated to stratification or terrigenous input and was likely driven to turnover in phytoplankton community

Abstract

The Chicxulub impact caused a crash in export productivity in much of the world's oceans which contributed to the extinction of 75% of marine species. In the immediate aftermath of the extinction, local export productivity was highly variable, with some sites, including the Chicxulub crater, recording elevated export production. The long-term transition back to more stable export productivity regimes has been poorly documented. Here, we present elemental abundances, foraminifer and calcareous nannoplankton assemblage counts, total organic carbon, and stable carbon isotopes from the Chicxulub crater to reconstruct long-term changes of productivity over the first 3 Myr of the Paleocene. We show that export production was elevated for the first 320 kyr of the Paleocene and then declined over the next ~900 kyr, remaining low thereafter. This interval is associated with fluctuations in water column stratification and terrigenous flux, but these variables are uncorrelated to export productivity. Instead, we suggest that the turnover in the phytoplankton community from a post-extinction assemblage dominated by picoplankton (which promoted nutrient recycling in the euphotic zone) to a more normal Paleocene pelagic community dominated by calcareous nannoplankton (which more efficiently removed nutrients from surface waters and led to oligotrophy) is responsible for the decline in export production in the southern Gulf of Mexico.

Plain Language Summary

The end Cretaceous mass extinction was caused by the impact of an asteroid on what is today the Yucatán Peninsula, Mexico. The impact ejected aerosols and dust into the air that reduced sunlight transmission, causing a severe decline in photosynthesis and the collapse of marine food webs. However, the change in the amount of food created by photosynthesizing plankton that makes it to the seafloor (export productivity) was variable across the oceans. At some places, including the Chicxulub crater, export productivity was actually high immediately after the impact. We produced a ~3 million year record of export productivity in the crater to determine how long it remained elevated and why it eventually declined. Export production was very high for the first 320,000 years after the impact and remained elevated for the next 900,000 years. We found that this production was not related to the input of nutrients via rivers around the Gulf of Mexico or how stratified the ocean was, but was probably driven by the change in the cell size of phytoplankton and its impact on export over the first million years of the Paleocene.

Keywords: K-Pg, Chicxulub Crater, Paleoproductivity, Foraminifera, Nannoplankton, Paleocene

1. Introduction

At the end of the Cretaceous Period (66.0 Ma), the impact of an asteroid on the Yucatán carbonate platform in the southern Gulf of Mexico caused the extinction of 75% of marine species (Alvarez et al., 1980; Smit et al., 1980; Hildebrand et al., 1991; Jablonski, 1995; Schulte et al., 2010), including ~90% of pelagic calcifiers such as planktic foraminifera and calcareous nannoplankton (Bown, 2004; Fraass et al., 2015; Lowery et al., 2020). Dust and sulfate aerosols ejected from the evaporite-rich carbonate target rock and soot from widespread wildfires blocked the sun, resulting in severe short-term cooling (Wolbach et al., 1985; Pope et al., 1994; Vellekoop et al., 2014, 2016; Bardeen et al., 2017 Brugger et al., 2017; Artemieva et al., 2017; Gulick et al., 2019; Artemieva and Morgan, 2020) and collapse of the food chain due to a sharp decline in photosynthesis (Zachos et al., 1989; D'Hondt et al., 1998; Kring, 2007). These effects were short-lived, however, as most dust, soot, and aerosols were removed from the atmosphere on the order of years (Brugger et al., 2017; Tabor et al., 2020), and the

oceans quickly became hospitable for life, even at ground zero in the Chicxulub crater (Lowery et al., 2018). Recent work quantifying oceanic pH changes across the K-Pg boundary has shown that post-impact ocean acidification lasted for ~ 40 kyr, and returned to pre-event values within 80 kyr, after a period of overshoot (Henehan et al., 2019). Meanwhile, temperature proxies and modelling data indicate that Deccan volcanism in the early Paleocene was insufficient to negatively impact early recovery ecosystems (Hull et al., 2020).

Given the short duration of adverse environmental conditions in the earliest Paleocene, it is puzzling that global marine productivity took at least 1.8 myr to recover to pre-extinction levels (e.g., Hsü and McKenzie, 1985; Zachos et al., 1989; D'Hondt and Zachos, 1998; Coxall et al., 2006; Birch et al., 2016). The collapse of export productivity at the K-Pg boundary has been observed via the vertical gradient of $\delta^{13}C$ between the surface ocean and seafloor. Under normal conditions, the sinking of ^{12}C-enriched organic carbon (termed the "biological pump" and primarily driven by the sinking remains of dead plankton) from the euphotic zone to the deep sea leaves the surface ocean enriched in ^{13}C and the seafloor depleted in ^{13}C. The post-K-Pg collapse in this gradient can be explained by a 50% reduction in the amount of organic matter exported from the euphotic zone (D'Hondt et al., 1998; Alegret et al., 2012; Henehan et al., 2019) or less, if part of the signal is from extinction-related changes in planktic foraminifer shell geochemistry (e.g., the extinction of photosymbiont-bearing planktics; Alegret et al., 2012; Birch et al., 2016). However, the exact mechanisms which controlled the eventual recovery of productivity and the relationship between the recovery of export production and the recovery of marine ecosystems remain unclear.

While carbon isotopes record the global average change in the strength of the biological pump, biogenic barium is a paleoproductivity proxy which correlates with local organic matter flux from overlying surface water (e.g., Griffith and Paytan, 2007). Barium proxy data indicates that export production did not uniformly decline across the oceans after the Chicxulub impact, as some sites actually show an increase (Hull and Norris, 2011). Broadly, sites from a range of water depths in the Gulf of

Mexico/North Atlantic/Tethys region record reduced export production in the early Danian (Alegret et al., 2001; Esmery-Senlet et al., 2015; Vellekoop et al., 2017), whereas sites in the central Pacific record increased export production during the same time period (Hull and Norris, 2011). A new earliest Danian record from the peak ring of the Chicxulub crater at International Ocean Discovery Program (IODP) Site M0077 revealed that the crater itself experienced high export productivity within foraminifer biozone Pα, within a few 10s of kyrs of the impact (Lowery et al., 2018). However, it was unclear how long high export productivity persisted at ground zero or how it relates to global patterns of heterogeneous export production in the early Danian. Was this locality oceanographically pre-disposed to high export productivity, or did changing conditions eventually lead to a decline? If so, what conditions shifted to cause lower export production? Jones et al. (2019) found that calcareous nannoplankton "disaster assemblages" persisted in the crater for approximately 1 myr post impact, well after they were replaced by incoming Paleocene taxa at other sites. Interestingly, the turnover from disaster assemblages to a succession of acmes of novel Paleocene nannoplankton species in the crater is associated with a shift in surface waters from eutrophic to oligotrophic conditions (Jones et al., 2019). Jones et al. (2019) speculated that these changes in the populations of primary producers are related to changes in export productivity, but lacked the data to test this, or determine what may have caused those changes.

Here, we compare the calcareous nannoplankton record of Jones et al. (2019) to planktic and benthic foraminifera, and major, minor, and trace elements to reconstruct export productivity, water column stratification, terrigenous flux, and phytoplankton population change during the early Paleocene interval (66.0-62.5 Ma) of IODP Site M0077 in the Chicxulub crater (Figure 1) in order to document the overall paleoceanographic evolution of the Chicxulub crater and to determine how long export production remained elevated after the K-Pg boundary. We then evaluate two competing hypotheses about the causes of the eventual decline in export production: environmental changes in the southern Gulf of Mexico or changes in the plankton ecosystem.

2. Material and Methods

In 2016, IODP/ICDP Expedition 364 drilled the peak ring of the Chicxulub crater (Morgan et al., 2017), coring over 100 m of post-impact Paleogene sediments with nearly 100% recovery. Ten meters of Paleocene pelagic carbonates were recovered at the base of the post-impact section, conformably overlying the top of the impact breccia. The uppermost 40 cm of these pelagic carbonates is cut by three disconformities and spans the middle and late Paleocene; the rest of the section, the focus of this study, spans the earliest to middle Paleocene, and is continuous from 66 to ~62 Ma (Morgan et al., 2017).

2.1 Microfossils

Samples for foraminiferal analysis were crushed with mortar and pestle into mm-sized pieces and then soaked in a solution of peroxide and borax for at least one week. They were then sieved over a 45 μm mesh to ensure recovery of generally small Paleocene taxa (care was taken to avoid juveniles in the counts, but many mature specimens – i.e., with multiple whorls – smaller than the more common 63 μm cutoff were present). The sieve was soaked in methylene blue dye between samples to identify any contamination. Sieved samples were dried in an oven and then split in a microsplitter to obtain a manageable number of foraminifera. At least 300 individuals were picked per sample. Additional specimens were extracted using a solution with 80% acetic acid and 20% H_2O, following the procedure of Lirer (2000). The best-preserved of these were imaged with the Zeiss MERLIN Field Emission Scanning Electron Microscope (FESEM) at the Universidad de Zaragoza.

2.2 XRF Core Scanning

Split cores were scanned with an AVAATECH XRF Core Scanner II at the University of Bremen. The split core surface was covered with a 4-μm thick SPEXCerti Prep Ultralenel foil to avoid contamination of the core material. Data were collected with a Canberra X-PIPS Silicon Drift Detector (Model SXD 15C-1150-500) with a 1550 eV X-ray resolution, the Canberra Digital Spectrum Analyzer DAS 1000, and an Oxford Instruments 50W XTF5011 X-Ray tube with rhodium target material, and ray data were processed using the iterative least squares software WIN AXIL from Canberra Eurisys. To

obtain sufficient resolution, we used a slit-size of 12 mm and a step-size of 10 mm. We conducted three line-scans to determine a range of element concentrations across the core section. For the first scan, we used an accelerating voltage of 50 kV and a beam current of 1 mA with a sampling time of 20 seconds to determine the concentrations of Ba and Sr. For the second scan, we used an accelerating voltage of 30 kV and a beam current of 1 mA with a sampling time of 20 seconds to determine the concentrations of Sr, Rb, Zr, Zn, Pb, and Ni. For the third scan, we used an accelerating voltage of 10 kV and a beam current of 0.15 mA with a sampling time of 20 seconds to determine the concentrations of Al, Si, K, Ca, Ti, Fe, Mn, and S. Ba, Ti, Al, Fe, and Ca scans are reported here.

2.3 Total organic carbon

Total organic carbon (TOC) was determined by measuring the difference between total carbon (TC) and total inorganic carbon (TIC). TC and TIC were determined via ignition and acidification, respectively, both of which produced CO_2 which was quantified with the infrared analyzer on an ELTRA CS500 carbon sulfur analyzer, with analytical error of <2%.

2.4 Carbon Stable Isotopes

Bulk rock samples were taken every 5 cm for stable isotope analysis at the Biogéosciences Laboratory, University of Bourgogne Franche-Comté, Dijon, France. Samples were crushed in an agate mortar and pestle into fine and homogeneous calcite powders, which were reacted with 100% phosphoric acid at 70°C using a ThermoScientific DELTA V PLUS mass spectrometer, connected to a Kiel IV carbonate preparation device. All isotopic values are reported in the standard δ-notation in per mil relative to VPDB (Vienna Pee Dee Belemnite) by assigning a $\delta^{13}C$ value of +1.95‰ to NBS19. External reproducibility as determined by replicate analyses of laboratory standards was ±0.04‰ (2σ) for carbon isotopes.

3. Results

3.1 Age Model

The age model used here (Table 1; Figure 2) is updated from the Expedition 364 Science Party (Gulick et al., 2017). Calcareous nannofossil taxonomy is based on the CP zonation scheme of Okada and Bukry (1980) following the taxonomic concepts of Perch-Nielsen (1985) and Bown (1998). Planktic foraminifer biostratigraphy is based on the P zones of Berggren and Pearson (2005) as modified by Wade et al. (2011), following the taxonomic concepts of Olsson et al. (1999) and Pearson et al. (2006). Key planktic foraminifer taxa are illustrated in Figure 3. Calibrated ages assigned to each datum are those reported in Appendix 3 of the Geologic Time Scale 2012 (Gradstein et al., 2012). Samples were taken at 2 cm increments from 616.2 -616.6 mbsf, and 5 cm increments above that. Paleomagnetic reversals are not included in the age model because a heterogenous chemical remnant re-magnetization occurred throughout the study interval obscuring the original polarity (Morgan et al., 2017; Gulick et al., 2019).

Although planktic foraminifera are abundant and diverse throughout the study interval, calcareous nannoplankton are rarer and much less diverse in the Paleocene interval of Site M0077, and form globally diachronous acmes for approximately 2 million years following the K-Pg mass extinction (Jones et al., 2019). Nannoplankton zonal markers at Site M0077 are either absent (tops of CP2 and CP3) or inconsistent with the planktic foraminifer datums (Tops of CP1 and CP4) (Figure 2). On the other hand, first and last occurrences of biostratigraphically significant planktic foraminifera taxa occur in the correct order and seem to indicate relatively constant sedimentation over the study interval (from the base of the Paleocene to planktic foraminifer biozone P2). Additionally, planktic foraminifer acme events (e.g., Arenillas et al., 2000) also occur within the expected planktic foraminiferal biozones at Site M0077. For these reasons, we consider the nannofossil datums which do occur at Site M0077 to be unreliable for age control and did not include them in the age model. We are confident the first and last occurrence datums of planktic foraminifera in the Chicxulub crater are coeval with those in the global ocean, and thus we have used planktic foraminifer biozones listed in Table 1 to construct the age model.

3.2 M0077 Sedimentology and Terrigenous Flux

The Paleocene interval at Site M0077 is primarily pelagic carbonate with varying degrees of dilution by terrigenous material (Figure 4). Magnetic susceptibility is a common tool to determine the terrigenous component in pelagic carbonates (e.g., Liu et al., 2012), although without determining the source of magnetic signal it loses some nuance, and so we use elemental data to provide more detail. Iron is generally correlated with terrigenous flux, while calcium is primarily sourced from biogenic carbonate (Rothwell and Croudace, 2015). Both Fe and Ca are often used to infer carbonate dissolution in deep sea cores, particularly during the Paleogene, which was characterized by discrete episodes of CO_2 release, warming, and ocean acidification (Bralower et al., 2002; Edgar et al., 2007; Quillévéré et al., 2008; Coccioni et al., 2010). However, we conclude that Fe and Ca variations at Site M0077 are driven by changes in dilution rather than dissolution because: (1) the site is relatively shallow (~ 700 m) water depth in the Paleocene (Lowery et al., 2018), well above the early Paleocene lysocline; and (2), intervals of elevated Fe/depressed Ca do not correspond to intervals of reduced foraminifer preservation (Figure 5). Core material at Site M0077 is strongly lithified, and had to be broken down with a mortar and pestle prior to soaking. An unfortunate side effect of this aggressive disaggregation is the fracturing of some portion of the foraminiferal tests. We did not distinguish foraminifera broken in this way from fragments of foraminifera which may have experienced partial dissolution on the seafloor due to deposition below the lysocline, a common proxy for ocean acidification ("Foram Fractionation Index;" Thunell 1976). In order to establish some quantitative proxy for foraminifer preservation, we instead report the number of individuals in each counted population that could not be identified to the genus level. These "planktic spp." are excluded from population analysis (other than planktic/benthic ratio) but provide a useful approximation of preservation, with more unidentifiable individuals indicating worse preservation. Figure 5 shows the lack of correlation between foraminifer preservation and Fe and Ca, and thus we interpret variations in Fe as a proxy for terrigenous flux and not dissolution. Additionally, Ti/Al ratios are often used to determine the relative contributions of fluvial and aeolian processes, as Ti is often associated with coarser size fractions delivered by fluvial processes and Al with small, clay-sized material blown to sea as dust (e.g., Ziegler et al., 2009; Govin et al., 2012).

Large variations in terrigenous flux are evident in the Paleocene interval of Site M0077 (Figure 4). Overall, terrigenous flux was low for the first ~ 1 Myr of the Danian and higher thereafter. Numerous shorter peaks are superimposed on this long-term trend. The base rate of terrigenous flux, particularly measured in Fe, is very low below 615.6 mbsf (65.4 Ma), has an initial peak at 615.0 mbsf (65.2 Ma), decreases somewhat, and then remains relatively elevated for the rest of the study interval. It should be noted that the closest land was > 500 km to the west in modern central Mexico (Gulick et al., 2019), and thus terrigenous material only slightly diluted the pelagic carbonate at Site M0077. Ti/Al is positively correlated with Fe (Figure 4), indicating that intervals of increased terrigenous flux to Site M0077 were driven by periods of enhanced fluvial input to the Gulf of Mexico. Thus, changes in terrigenous flux are a useful proxy for changes in continental weathering in the Gulf of Mexico basin.

3.3 Water Column Structure

Planktic foraminiferal paleoecology provides insight into local hydrography. Planktic foraminifera occupy specific depth habitats in open ocean environments which can be determined via single-species isotopic analysis (e.g., Aze et al., 2011; Birch et al., 2012). The pervasive foraminiferal recrystallization throughout Site M0077 prevents this kind of geochemical analysis, but fortunately we can use the Paleocene compilation of Aze et al. (2011) and other published records to assign the species to depth habitats (Table 2). The use of planktic foraminifer populations to reconstruct water column stratification is fairly common, particularly the relative abundance of deeper dwelling taxa (e.g., Leckie et al., 2002; D'Onofrio et al., 2016; Lowery et al., 2020). Here, we use the relative proportion of mixed layer, thermocline, and sub thermocline taxa to reconstruct the degree to which the water column was stratified (Figure 6). Dominance of mixed layer taxa indicates the lack of suitable habitat for thermocline/subthermocline species, suggesting weak stratification with the mixed layer habitat extending through much of the photic zone. Higher abundances of thermocline and subthermocline taxa indicate a more stable habitat for these species, which may result from stronger water column stratification.

Conversely, a dominance of mixed layer taxa may indicate a lack of strong vertical stratification with no habitat for organisms which live below stratified layers.

Overall, Site M0077 is dominated by mixed layer taxa for the first ~ 200 kyr of the Danian, followed by a shift to more stratified waters from ~ 200-400 kyr (616.3-615.9 mbsf) after the boundary, a return to mixed-layer dominated waters from 400-900 kyr (615.9-614.9 mbsf) after the boundary, and finally a more permanent shift toward stable stratified waters after 900 kyr (above 614.9 mbsf) (Figure 6). Schaefer et al. (2020) found biomarker evidence for intermittent photic zone euxinia beginning around 1 myr after the K-Pg boundary, just above the level where we find the final shift to stable stratified waters. Photic zone euxinia implies a lack of downward mixing of oxygenated surface waters, providing additional evidence for increased stratification. The lack of evidence for photic zone euxinia below this level suggests that poor stratification eliminated habitat space for thermocline and subthermocline species in intervals dominated by mixed layer taxa.

3.4 Export Productivity

Export production, the removal of organic matter from the euphotic zone to the deep sea, is primarily driven by the biological pump, in which organic matter is moved downward via biological pathways like sinking, fecal pellets, the daily vertical migration, etc. (Zhang et al., 2018). The pump is usually described as having two parts: the export of net primary production out of the euphotic zone (~ 100 m depth) and the scavenging and remineralization of that organic carbon as it sinks to the seafloor, or at least deep enough to be removed from the short-term carbon cycled (~ 1000 m depth) (e.g., Boyd and Newton, 1995; Buessler, 1998; Legendre and Rivkin, 2002; Boyd and Trull, 2007; Buessler and Boyd, 2009; Henson et al., 2012). The amount of organic matter exported from the euphotic zone is often referred to as “export efficiency” (e.g., Buessler and Boyd, 2009) or pump “strength” (e.g., Henson et al., 2012), and the amount of organic matter that sinks below 1000 m is called “transfer efficiency” (Buessler and Boyd, 2009) or pump “efficiency” (Henson et al., 2012); we opt to use strength vs. efficiency here

(Henson et al., 2012). In the modern ocean these variables can be directly measured via satellites and water sampling, but in paleoceanographic studies we can only indirectly reconstruct export production via sedimentary proxies.

Biogenic barium, primarily preserved in marine sediments as barite ($BaSO_4$), strongly correlates with modern export production (Dymond et al., 1992; Francois et al., 1995; Eagle et al., 2003; Paytan and Griffith, 2007) and is thus a commonly used export productivity indicator (e.g., Payton et al., 1996; Bains et al., 2000; Griffith and Paytan, 2012). Barite is primarily formed in marine environments during the remineralization of sinking organic matter, but it can also be sourced from terrigenous sediments. Therefore, barium is normalized to the terrestrially-sourced element titanium (Dymond et al., 1992; Paytan and Griffith, 2007). This "excess barium" proxy has been used to reconstruct export production in the early Paleocene using XRF data (Hull and Norris, 2011), as we do in this study. Different continental drainage basins may have differing Ba/Ti ratios, and thus long-term changes in sediment source area or dust vs. riverine flux may complicate interpretation of export productivity (Payton and Griffith, 2007). However, significant changes in the sediment source to the southern Gulf of Mexico did not occur until the Laramide Orogeny, which began in the late Paleocene and therefore would not have influenced early Paleocene sedimentation (Galloway et al., 2000). Shorter term sedimentation changes related to impact-driven land denudation (e.g., Tschudy et al., 1984) were on the order of 8-20 kyr (Vajda et al., 2004), too brief to explain the trends we observe. Because sediment is exclusively pelagic limestone, we consider sedimentary source changes to be an unlikely driver of observed trends in biogenic barium. Another possible source of barium in our study area is from the crater hydrothermal system, which was active throughout our study interval, and which caused the precipitation of secondary barite in pore fluids in the underlying impact breccia (Kring et al., 2020). We also regard this as an unlikely source of Ba enrichment in the pelagic Paleocene sediments we examine here because secondary barite is only observed in the impact breccia, meters below the contemporary Danian seafloor (Kring et al., 2020). Additionally, Ba is only enriched in the lower few meters of the post impact sediments, while other hydrothermal elements

are enriched throughout our study interval, indicating that the hydrothermal system was active for millions of years after the crater formed (Kring et al., 2020) and that Ba was not supplied to the seafloor by this mechanism.

While Ba/Ti ratios can tell us about the overall strength and efficiency of the whole biological pump, foraminifer ecology can help us understand some of its component parts. Planktic foraminifera live in the upper water column and record conditions related to primary production. Paleocene planktic foraminifer taxa exhibit adaptations which allows them to make some groups better adapted to different levels of primary productivity. In the early Danian, some new genera (*Eoglobigerina* and the Subbotinids) evolved spines, long protrusions of calcite which provide an anchor for rhizopods (i.e., feeding appendages) and allow them to hold on to motile prey, enabling these groups to adapt a carnivorous lifestyle and graze upon other zooplankton (Hemleben et al., 1991; Olsson et al., 1999). On the other hand microperforate and smooth normal perforate planktic foraminifera (in the Paleocene, these include *Guembelitria, Globoconusa, Parvularugoglobigerina, Woodringina, Chiloguembelina,* etc.) are unable to eat zooplankton, which are generally able to free themselves from unsupported rhizopodal networks; these foraminifera are primarily grazers, feeding on phytoplankton and any organic detritus that drifts by (Hemleben et al., 1991). In the modern ocean, photosymbiont-bearing planktic foraminifera tend to dominate in oligotrophic subtropical gyres (e.g., Hemleben et al., 1991). Photosymbiosis existed in planktic foraminifera in the Cretaceous but all those groups went extinct at the K-Pg boundary, and the strategy re-evolved several million years later at the end of our study interval, beginning with *Praemurica inconstans* and followed by *Acarinina, Morozovella,* and *Igorina* (Norris, 1996; Birch et al., 2012). Spinose and symbiont-bearing planktic foraminifera are better adapted to food-limited environments, and should be predominant in oligotrophic waters. On the other hand, non-spinose, non-symbiont bearing planktics, the grazers, are best adapted to eutrophic environments, and should be dominant there.

Benthic foraminifera are also powerful paleoenvironmental indicators. They are primarily sensitive to changes in dissolved oxygen and food supply (Jorissen et al., 1995; Gooday, 2003; Van

Hinsbergen et al., 2005), and benthic abundance is also often inversely correlated with water depth (e.g., Murray, 1976; Culver, 1988; Van der Zwaan et al., 1990; Leckie and Olson, 2003). The seafloor at Site M0077 was clearly well-oxygenated throughout the study interval as evidenced by abundant ichnofauna (Morgan et al., 2017; Rodriguez Tovar et al., *in press*) due to the lack of a crater wall to the northeast (Gulick et al., 2008). The site was located in upper/middle bathyal depths (600-700 m; Gulick et al., 2008; Lowery et al., 2018), and low-amplitude sea level change throughout the early Paleocene (e.g., Miller et al., 2020) should not have affected the %benthics at this depth. With changes in oxygen and sea level thus ruled out, we are confident that food supply to the seafloor (i.e., export production) was the strongest influence on %benthics at Site M0077. %Benthics may reflect changes in either the quantity or the quality (i.e., labile vs. refractory) of the organic matter that reached the seafloor (e.g., Jorissen et al., 1995).

Export productivity, measured by Ba/Ti, was high overall in the early Danian, and broadly declined from 66.0 to ~64.5 Ma (616.5 to ~613.7 mbsf) (Figure 6). The interval of highest export productivity terminated sharply around 65.7 Ma (616.2 mbsf). The subsequent period of decline is interrupted by a second peak in export production which occurred around 65.2 Ma (615.1 mbsf), after which export production flattens out. The initial ~1 Myr period of high, generally declining export productivity is also reflected in the foraminifera populations. Benthic foraminifera are more abundant overall in the early Danian (Figure 6), indicating either higher export of organic matter to the seafloor overall or a relatively large proportion of labile organic matter being exported. Likewise, non-spinose, non-symbiont-bearing planktic foraminifera are more abundant in the early Danian as well (Figure 6). This dominance is not an artifact of post-extinction communities being composed of only non-spinose foraminifera. Spinose foraminifera appeared essentially immediately after the extinction: the lowest occurrences of *Eoglobigerina* and *Parasubbotina* occurs in Zone P0, while that of *Subbotina* occurs early in Zone P1a, ~300 kyr after the boundary, indicating that an evolutionary advantage conferred by spines existed in at least some parts of the ocean soon after the impact. The fact that the multiple existing species of spinose foraminifera in the Chicxulub crater were out-competed by non-spinose foraminifera suggests

that spines did not confer much of an advantage at this *particular* place and time, which indicates food must have been plentiful. Although not directly correlated with export productivity as measured by Ba/Ti, these foraminifer proxies provide additional context on the state of different aspects of the biological pump. Calcareous nannoplankton abundance data (Figure 6) show that the interval of overall high productivity was dominated by calcareous nannofossil "disaster taxa" which bloomed in the aftermath of the K-Pg mass extinction (Jones et al., 2019). These taxa persist longer at Chicxulub (~ 1 myr) than any of the other sites.

The rest of the study interval is characterized by low and stable Ba/Ti ratios (with several small short-lived increases), higher abundances of oligotrophic planktic foraminifera, and fewer benthic foraminifera. As export productivity entered the last stages of its decline, the calcareous nannoplankton assemblage becomes more diverse, with the onset of a series of acme events, dominated by increasingly oligotrophic taxa (Jones et al., 2019).

4. Paleoceanographic evolution of the Chicxulub Crater

Collectively, our data indicate a shift from high export productivity and weak stratification in the earliest Paleocene to low export productivity and strong stratification a few million years later. The change between these two regimes also marks a shift in the plankton community. This progression occurs in several steps (see numbered, shaded bars on Figure 6) detailed below.

4.1 High export productivity, well-mixed water column (66.0-65.9 Ma).

The first 100 kyr after the Chicxulub impact (616.5-616.4 mbsf) were characterized by high export production and were dominated by mixed-layer planktic foraminifera, predominantly *Guembelitria*, *Globoconusa*, and *Parvularugoglobigerina*, while the disaster taxon *Cervisiella* dominated the nannoplankton community. Schaefer et al. (2020) used biomarkers to document a bloom of cyanobacteria in this interval as well. Several acmes of planktic foraminifera occurred across the Tethys and North Atlantic after that K-Pg boundary, termed Planktic Foraminiferal Acme Stages (PFAS;

Arenillas et al., 2000, 2006, 2016; Alegret et al., 2004). These represent a coeval succession of dominant taxa in open marine sections over a wide geographic area. PFAS-1, the predominance of *Guembelitria*, occurs in this earliest interval of post-impact sedimentary rocks (Figure 7).

4.2 Very High export productivity, increasing stratification (65.9-65.7 Ma).

During the period from 100-320 kyr after the impact (616.4-616.1 mbsf), export productivity peaked, benthic foraminifer abundance increased, and thermocline and sub-thermocline dwelling foraminifera (*Eoglobigerina* and *Chiloguembelina*) became more common. This transition is coincident with a small increase in terrigenous flux (Figure 4). PFAS-2, the predominance of *Globoconusa* and *Parvularugoglobigerina*, occurs in this interval (Figure 7). The nannoplankton assemblage was still dominated by the calcareous resting cysts of dinoflagellates (*Cervisiella*).

4.3 Declining export productivity, well stratified water column (65.7-65.6 Ma).

A sharp decrease in export productivity occurred ~320 kyr after the boundary (616.1 mbsf) in the middle of a period of well-developed water column stratification. *Braarudosphaera* became predominant in the nannofossil assemblage as *Cervisiella* declined, but this is coincident with an increase in foraminifer-sized calcispheres tentatively identified as *Cervisiella* (Figure 6), suggesting that this taxon may have just grown to a larger size because of a shift to particularly suitable conditions. Lieberand et al. (2017) found *Braarudosphaera* oozes associated with hyperstratification during during the Oligocene. This matches with increase in stratification we observe with planktic foraminifera at Site M0077. PFAS-3, the predominance of *Woodringina* and the sub-thermocline-dwelling *Chiloguembelina*, also begins in this interval. This correlation, and the brief nature of this event, suggests that the changes in stratification observed at Site M0077 are part of larger trends that extend at least across the North Atlantic. The Dan-C2 hyperthermal, which is not recorded in our carbon isotope data but which occurred at 65.7 Ma across the North Atlantic (e.g., Quillévéré et al., 2008; Barnet et al., 2019), may have caused an increase in thermal stratification. A reduction in latitudinal temperature gradients during warm periods could have

reduced circulation and increased stratification. The lack of the diagnostic isotope excursion for this event at Site M0077 may be due to a combination of low sedimentation rate and pervasive bioturbation combined with diagenetic alteration of the carbonate; there is no evidence for a hiatus at this level. This interval is not associated with any evidence for increased terrigenous flux.

4.4 Moderate export productivity, poorly stratified water column (65.6-65.1 Ma).

400 kyr after the impact (615.9 mbsf), water column stratification weakened and mixed layer taxa again dominated the planktic foraminiferal assemblage. Benthic foraminifera reached their peak abundance, perhaps indicating an increase in labile organic matter arriving at the seafloor. Foraminifer-sized calcispheres peaked and then declined as *Cervisiella* again came to dominate the nannofossil assemblage (Jones et al., 2019). Export productivity had declined from its earlier peak but was still relatively elevated compared to subsequent values.

4.5 Stratification redevelops and productivity bottoms out (65.1-64.7 Ma)

Over the next ~ 400 kyr (614.9-614.1 mbsf) stratification gradually strengthened while export productivity slowly declined following a final large peak just below this interval. The termination of this peak is associated with the onset of the first bloom of incoming Paleocene nannoplankton, *Futuyania petalosa*, at the very base of this interval, 900 kyr after the K-Pg boundary (Jones et al., 2019). This taxon becomes more abundant throughout this interval, in conjunction with a small peak in the Ba/Ti ratios indicating export production that was lower than before but still higher than what is to come. Declining export productivity is associated with an increase in spinose foraminifera, which have a broader diet than non-spinose, non-symbiont-bearing planktics and thus were (and still are) better suited for lower nutrient waters (e.g., Hemleben et al., 1991).

Total organic carbon is essentially zero for the first million years of the Danian and is higher, although still low, from 65.0-62.5 Ma (Figure 6). TOC enrichment is controlled by both productivity and preservation (e.g., Pederson and Calvert, 1990), so an increase in TOC concurrent with a reduction in

export productivity suggests an increase in the preservation potential of organic matter. The most likely mechanism for this increase is reduced ventilation of the seafloor, suggesting enhanced stratification at the study area after 65.0 Ma. Biomarker data indicate the development of intermittent photic zone euxinia in the crater at this time, providing additional evidence for increased stratification (Schaefer et al., 2020). This interval is concurrent with increasing terrigenous flux (Figure 5).

4.6 Stable, Stratified Water Column, Low Export Productivity (64.7-62.6 Ma)

The rest of the lower Paleocene record at Site M0077 (614.1-610.6 mbsf), below a series of stacked unconformities spanning the uppermost Danian to the PETM, documents a stable, stratified, increasingly oligotrophic environment. A stepped decline in Ba/Ti at the base of this interval is associated with the initiation of the acme of *Cruciplacolithus primus* and then *Coccolithus pelagicus* (Jones et al., 2019). Following the *Praeprinsius* acme, which terminates around 63.5 Ma (Jones et al., 2019), no further acmes occur, indicating that the post-extinction ecosystem was finally stabilized. Ba/Ti ratios are essentially stable although increase slightly through this interval.

5 What Drove the Decline in Export Production?

A clear change in export productivity occurs ~300 kyr after the K-Pg boundary at many sites around the globe, although with local differences in whether export production goes up or down. In the western Gulf of Mexico, benthic foraminiferal assemblages indicate an increase to pre-extinction levels of export production ~300 kyr post impact (Alegret et al., 2001; Alegret and Thomas, 2005). Benthic foraminifer assemblages document a similar increase ~300 kyr after the K-Pg boundary on the eastern side of the Atlantic Ocean in Spain (Alegret and Thomas, 2005). At the Gubbio section in Italy there is an increase in benthic foraminifer abundance around 300 kyr after the boundary, suggesting higher export productivity (Coccioni et al., 2010). At Maud Rise in the Southern Ocean, Ba/Ti and Ba/Fe ratios begin to rise ~300 kyr after the K-Pg boundary (Hull and Norris, 2011). At Shatsky Rise in the equatorial Pacific, export productivity briefly increases ~300 kyr after the K-Pg (Hull and Norris, 2011). Birch et al. (2016)

found an initial recovery of export productivity ~ 300 kyr after the boundary at Walvis Ridge in the South Atlantic. These sites are broadly distributed geographically, and represent a range of depositional environments. Although there are other sites at which no change is observed at this point in time (e.g., Vigo Seamount, São Paulo Plateau, and Wombat Plateau; Hull and Norris, 2011), the lack of a globally consistent shift in productivity may be considered analogous to other major paleoceanographic events, like the Paleocene Eocene Thermal Maximum (e.g., Gibbs et al., 2006) or Oceanic Anoxic Event 2 (Tsikos et al., 2004), in which local signals often differ significantly from the global "average" change.

These widespread shifts in export productivity around 65.7 Ma could be driven by a shift in ocean circulation patterns driving a shift in thermal stratification and mixing processes which reduced nutrient delivery to the euphotic zone. Indeed, there are limited data in support of changes in stratification at this time, including at Walvis Ridge in the South Atlantic (Birch et al., 2016) and the Gubbio section in Italy (Coccioni et al., 2010).

An alternative explanation is that shifts in export production are part of the gradual recovery of marine ecosystems after a major mass extinction event. In this hypothesis, changes in the plankton ecosystem drove changes in the local biological pump and explain regional patterns of export productivity change. Plankton ecology is the single most important control on the strength and efficiency of the biological pump (e.g., Henson, 2012). In the modern ocean, net primary production (NPP) driven by large celled phytoplankton like diatoms and coccolithophores results in a stronger biological pump and thus higher export production (e.g., Boyd and Newton, 1995, 1999; Buessler, 1998; Legrende and Rivkin, 2002; Boyd and Trull, 2007; Lam et al., 2011; Boyd, 2015). Primary production by smaller-celled picophytoplankton like algae and cyanobacteria sinks more slowly and is more easily remineralized in surface waters (the "microbial loop"); in regions where picoplankton dominate primary production, nutrients are constantly recycled at shallow depth and export production is primarily composed of more refractory organic matter which is resistant to degradation (Legrendre and Michaud, 1998; de la Rocha and Passow, 2007). Counter intuitively, even though the biological pump is weaker when primary

production is dominated by picoplankton (less organic matter is exported from the euphotic zone), it is more efficient (a larger proportion of the organic matter that is exported from the euphotic zone safely sinks to the seafloor because it is more refractory). This is because even though larger celled phytoplankton tend to sink more quickly, they don't sink quickly enough to avoid scavenging at intermediate depths, so the abundance of larger phytoplankton has the net effect of removing organic matter and nutrients from the euphotic zone but not exporting it efficiently to the seafloor. For example, Henson et al. (2012) document a strong, inefficient biological pump at high latitudes driven by diatoms, in which 15-25% of NPP sinks below the euphotic zone but only 1-10% of that material reaches 2000 m water depth (where it is considered "exported," i.e., removed from the short term carbon cycle). On the other hand, they describe a weak, efficient pump at low latitudes driven by small-celled phytoplankton, where only 1-5% of NPP makes it out of the euphotic zone but 20-35% of that makes it to 2000 m.

After the K-Pg mass extinction, the dominant larger-celled phytoplankton of the Cretaceous, calcareous nannoplankton, declined severely. Primary production was carried on by picoplankton like chlorophyte algae (Sepúlveda et al., 2009) and cyanobacteria (Schaefer et al., 2020; Bralower et al., *in revision*), weakening the biological pump. In some oligotrophic regions, the shift toward picoplankton and enhanced recycling of nutrients in the euphotic zone may have actually driven a local increase in primary productivity (see discussion in Henehan et al., 2019). If the southern Gulf of Mexico was one of these regions, then the recovery of calcareous nannoplankton would have facilitated a higher removal of nutrients from the euphotic zone, thus causing the observed local shift from eutrophic to oligotrophic conditions.

Thus we have two hypotheses to explain the early Paleocene export productivity data at Site M0077: 1) increasing stratification (driven either by changes in global circulation or the local hydrologic cycle) reducing nutrient availability, or 2) a recovery of larger celled phytoplankton increasing export of nutrients and organic matter from the euphotic zone, reducing nutrient availability. Testing the latter hypothesis would require data on the relative abundance of groups of phytoplankton which do not usually

leave body fossils, like algae and cyanobacteria, and such data does not currently exist for any K-Pg boundary section. Biomarker data from the Chicxulub crater do indicate a dominance of cyanobacteria in the first few 100 kyrs after the K-Pg Boundary (Schaefer et al., 2020), corresponding to the interval of the highest export production and thus providing some support for this idea. Bralower et al. (*in revision*) found evidence of global blooms of microbial phytoplankton associated with the widespread deposition of microcrystalline calcite above the K-Pg boundary. Moreover, Alvarez et al. (2019) found an increase in average nannoplankton cell size coincident with the initial increase in diversity at Shatsky Rise in the equatorial Pacific, indicating connection between nannoplankton cell size and the recovery of the biological pump. However, without detailed plankton biomarker data we only have an incomplete picture of the potential phytoplankton community and cannot directly test this hypothesis. We can, however, test the alternate hypothesis, that increasing stratification drove a decline in export productivity, by determining if there is a correlation between proxies for stratification and/or terrigenous flux and export productivity in the Chicxulub crater.

Figure 8 is a series of cross plots showing the lack of correlation between export productivity indicated by Ba/Ti ratios and proxies for stratification and terrigenous flux. Figures 8A and B compare two proxies for overall terrestrial input, total Fe and magnetic susceptibility, with export productivity; both clearly show no trend. Figure 8C compares the ratio of Ti to Al, which tracks shifts in aeolian vs. riverine input (e.g., Govin et al., 2012) with export productivity. There are clear shifts in the Ti/Al ratio (Figure 4) coincident with shifts in Ca and Fe, indicating that shifts between wetter and drier climate states drove changes in the delivery of terrigenous elements to Site M0077. However, when plotted against Ba/Ti, it is clear that such shifts in sediment source have no bearing on export productivity. But perhaps nutrients were sourced from depth, and there is a relationship between a weakly stratified water column (facilitating upwelling) and enhanced export production. Figure 8D compares the percentage of mixed layer planktic foraminifera with Ba/Ti to test this idea, and convincingly demonstrates that changing stratification was unrelated to export productivity.

We therefore conclude that changes in terrigenous flux and stratification did not affect early Paleocene export productivity in the southern Gulf of Mexico. We favor the hypothesis that turnover in phytoplankton communities from picophytoplankton like cyanobacteria to larger phytoplankton like coccolithophores drove a strengthening of the biological pump and, paradoxically, a reduction in the nutrients in the photic zone and thus a decline in export production. Biomarker-based studies of the whole plankton ecosystem from multiple early Paleocene sites are necessary to test this hypothesis.

6. Conclusions

The earliest Danian oceanic environment is often referred to as generally "unstable" (e.g., Hull et al., 2011). Our data suggest that at least one component of this instability is a fluctuating degree of water column stratification. Water column stratification varied widely over the first ~ million years of the Paleocene, but with an overall trend from poorly stratified to well stratified. Export productivity varied over the same interval, with an overall decreasing trend. There is no strong correlation between proxies for stratification or terrigenous flux with export productivity. Instead, we suggest that the decline in export productivity was linked to turnover in the phytoplankton community, as post-impact blooms of cyanobacteria (Schaefer et al., 2020; Bralower et al., *in revision*) and other non-fossilizing picophytoplankton gave way to larger calcareous nannoplankton. Picophytoplankton sink so slowly that they are generally completely remineralized in the euphotic zone, increasing nutrients there and ensuring that most organic export was highly refractory and thus likely to survive its trip to the seafloor. Larger celled phytoplankton sink more quickly, and thus remove more nutrients from the euphotic zone. However, this sinking is not fast enough to avoid scavenging below the euphotic zone, and the more labile organic matter is more easily remineralized as it sinks, resulting in lower overall export of organic carbon to the seafloor in regions not predisposed to high productivity. Existing data from Site M0077 support this plankton ecology hypothesis, with a dominance of cyanobacteria during the interval of highest export production, and recovery of calcareous nannoplankton diversity as export production

declines, but more complete biomarker data on the rest of the non-fossilizing phytoplankton ecosystem are required to truly test it.

Data Availability Statement

Planktic foraminifer data and XRF core scan data will be uploaded to the NOAA National Climate Data Center before publication. Calcareous nannoplankton data are from Jones et al. (2019) and are archived as GSA Data Repository Item 2019271.

Acknowledgements

We are grateful to Ellen Thomas, Julio Sepúlveda, and two anonymous reviewers for their constructive comments, which have substantially improved this work. The authors acknowledge NSF OCE 1737351, 1736951, and 1737199. We are grateful to Pincelli Hull for her helpful discussions on our data and hers, and to the staff of the Bremen Core Repository for their invaluable help sampling and scanning the core. We also thank Tessa Cayton for her assistance preparing foraminifer samples. I.A. and J.A.A. acknowledge the use of the Servicio General de Apoyo a la Investigación-SAI, Universidad de Zaragoza. The European Consortium for Ocean Research Drilling (ECORD) implemented Expedition 364 with funding from the International Ocean Discovery Program (IODP) and the International Continental scientific Drilling Project (ICDP). Data and samples can be requested from IODP. U.S. participants in Exp. 364 were supported by the U.S. Science Support Program. J.V.M. was funded by NERC, Grant: NE/P005217/1. I.A. and J.A.A. were supported by MINECO/FEDER-UE (project number CGL2015-64422-P) and MCIU/AEI/FEDER, UE (project number PGC2018-093890-B-I00). This is UTIG Contribution #3661.

Appendix 1

Expedition 364 Science Party: Elise Chenot, Gail Christeson, Philippe Claeys, Charles Cockell, Marco J. L. Coolen, Ludovic Ferrière, Catalina Gebhardt, Kazuhisa Goto, Sophie Green, Kliti Grice, Sean Gulick, Heather Jones, David A. Kring, Johanna Lofi, Christopher M. Lowery, Claire Mellett, Joanna Morgan, Rubén Ocampo-Torres, Ligia Perez-Cruz, Annemarie Pickersgill, Michael Poelchau, Auriol Rae, Cornelia Rasmussen, Mario Rebolledo-Vieyra, Ulrich Riller, Honami Sato, Bettina Schaefer, Jan Smit, Sonia Tikoo, Naotaka Tomioka, Jaime Urrutia-Fucugauchi, Michael Whalen, Axel Wittmann, Long Xiao, Kosei Yamaguchi, William Zylberman

Table 1. Biostratigraphic datums for the Paleocene interval of Hole M0077A. Nannofossil datums marked with asterisks are not used in the age model. Datum ages after Gradstein et al. (2012).

Taxon	Zone	Sample Above	Sample Below	**Avg. Depth**	**Datum Age**
Discoaster multiradiatus	Base of CP8	607.26	607.37	**607.315**	**57.21**
Morozovella acuta	Base of P4b	607.52	607.76	**607.65**	**57.79**
*Heliolithus kleinpellii**	Base of CP5	607.52	607.76	**607.65**	**59.94**
Igorina pusilla	Base of P3a	609.28	609.3	**609.29**	**62.3**
Praemurica uncinata	Base of P2	610.6	610.65	**610.63**	**62.6**
Globanomalina compressa	Base of P1c	612.36	612.41	**612.385**	**63.9**
*Chiasmolithus danicus**	Base of CP2	612.5	612.75	**612.625**	**64.81**
Subbotina triloculinoides	Base of P1b	615.21	615.26	**615.235**	**65.25**
Parvularugoglobigerina eugubina	Base of P1a	616.15	616.2	**616.175**	**65.72**
Parvularugoglobigerina eugubina	Base Pα	616.56	616.56	**616.56**	**66**

579 **Table 2.** Planktic foraminifer depth habitat assignments based on the ecogroups of Aze et al., 2011. All assignments are from that paper unless

580 otherwise noted. No taxa assigned to Groups 5 and 6 appear in our dataset.

Aze et al. 2011 ecogroups	Group	Explanation	Members
Group 1	Open ocean mixed-layer tropical/subtropical, with symbionts	Very heavy $\delta^{13}C$ and relatively light $\delta^{18}O$	*Morozovella, Igorina, Acarinina, Praemurica inconstans*~, *Preamurica pseudoinconstans*~, *Praemurica uncinata*~
Group 2	Open Ocean mixed-layer tropical/subtropical, without symbionts	$\delta^{13}C$ lighter than species with symbionts; also relatively light $\delta^{18}O$	*Guembelitria**, *Parvularugoglobigerina**, *Woodringina**, *Globoconusa daubjergensis**†, *Rectuvigerina cretacea**, *Praemurica taurica*, *Subbotina triangularis*,
Group 3	Open Ocean thermocline	Light $\delta^{13}C$ and relatively heavy $\delta^{18}O$	*Globanomalina, Eoglobogerina Parasubbotina varianta, Subbotina trivialis, Subbotina triloculinoides*
Group 4	Open Ocean sub-thermocline	Very light $\delta^{13}C$ and very heavy $\delta^{18}O$	*Chiloguembelina midwayensis**, *Chiloguembelina morsei*^, *P. pseudobulloides*
Group 5	High Latitude	Species only found in high latitude sites	N/A
Group 6	Upwelling/high productivity	Species only found in sites of high productivity or upwelling	N/A

*Olsson et al., 1999 and references therein

†Olsson (1999): "Although its abundance in near-shore sequences indicates a near-surface planktic habitat (Troelsen, 1957; Keller, 1989; Liu and Olsson, 1992), its oxygen isotopic signature and open-marine abundance patterns suggest a preference for relatively cool water masses (Premoli Silva and Boersma, 1989; D'Hondt and Keller, 1991; Liu and Olsson, 1992; D'Hondt and Zachos, 1993)."

~Norris (1996) and Birch et al. (2012) describe *P. inconstans, P. pseudoinconstans,* and *P. uncinata,* as symbiont-bearing.

^no isotope data are available for any other Paleocene Chiloguembelinids, so we place *Ch. morsei* in this group based on the data from its cousin *Ch. midwayensis.*

581

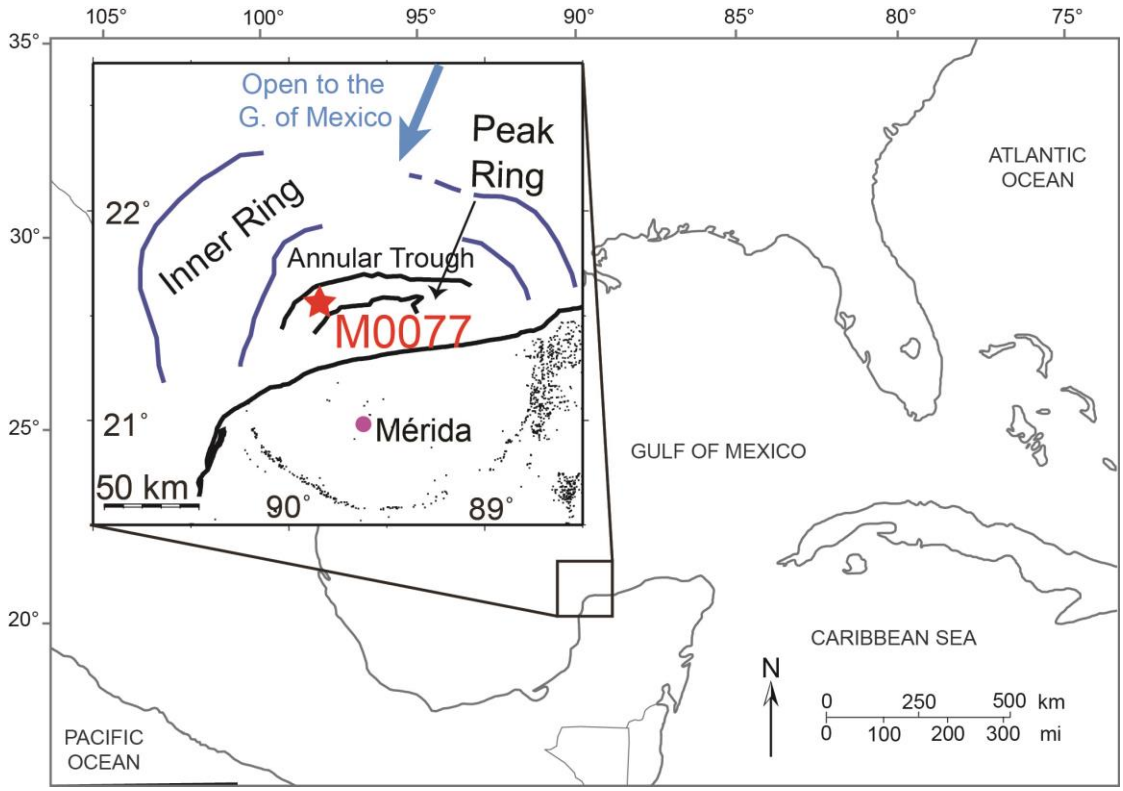

582

583 **Figure 1.** Location map showing the position of IODP Site M0077 within the Chicxulub crater.

584

585

586

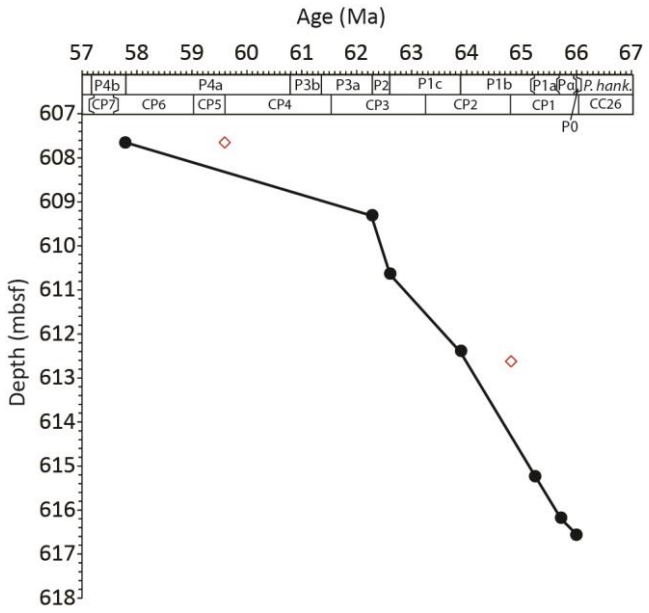

587

588 **Figure 2.** Age-Depth plot showing the construction of the age model. Black circles are planktic

589 foraminifer datums, open diamonds are calcareous nannoplankton, several of which are missing from this

590 core. P zones are planktic foraminifer and CP zones are calcareous nannoplankton. The study focuses on

591 the first ~3.5 myr of the Paleocene, to the base of Zone P2.

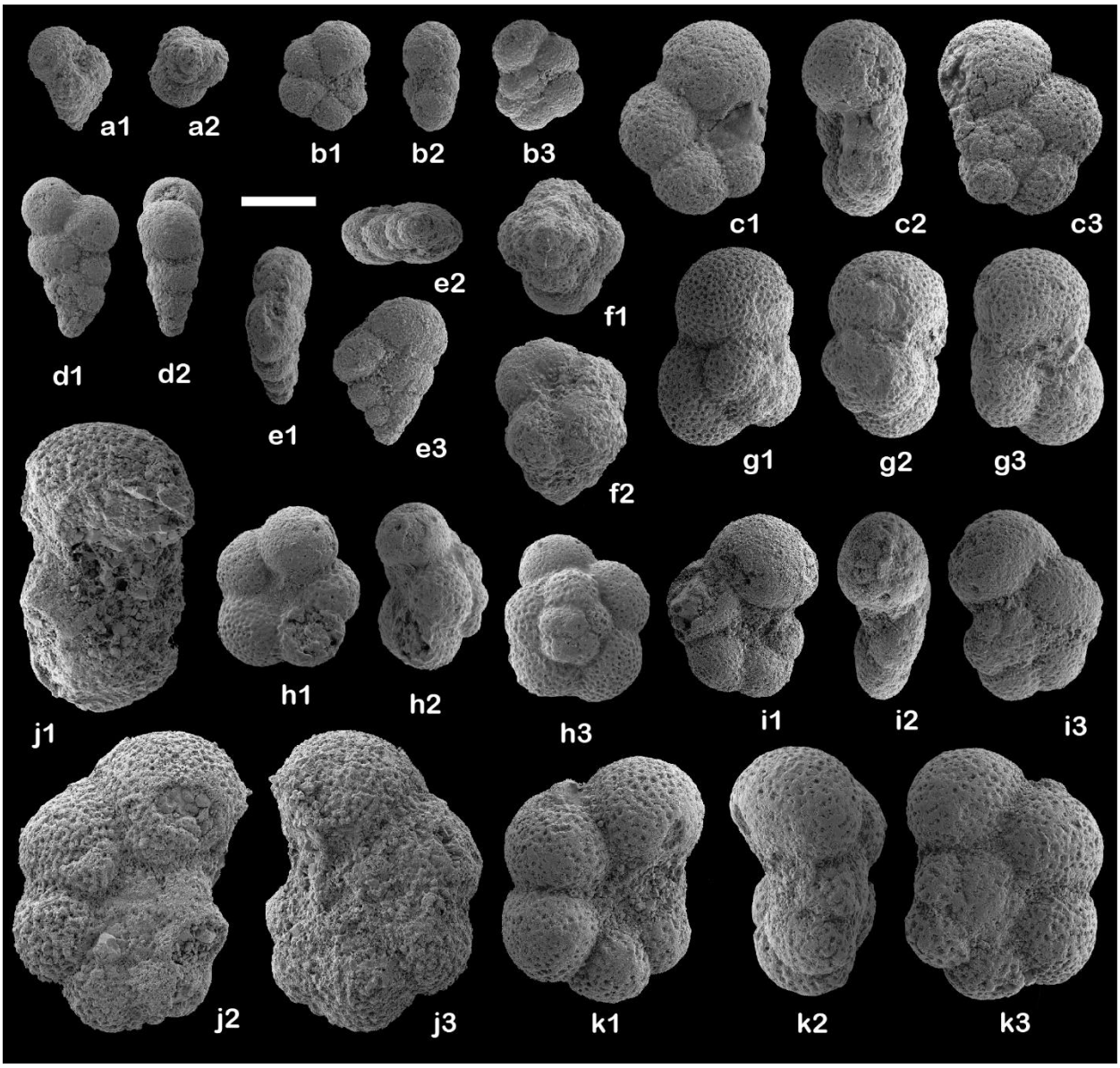

Figure 3. SEM images of planktic foraminiferal index-species and other relevant species (scale bar = 100 microns). (a) *Guembelitria cretacea* (364-M0077A-39R-2 85-86 cm); (b) *Parvularugoglobigerina eugubina* (364-M077A-40R-1 17-18 cm); (c) *Parasubbotina pseudobulloides* (364-M0077A-39R-1 128-129 cm); (d) *Chiloguembelina morsei* (364-M0077A-39R-2 98-99 cm); (e) *Chiloguembelina midwayensis* (364-M0077A-39R-3 41-42 cm); (f) *Globoconusa daubjergensis* (364-M0077A-37R-2 116-117 cm); (g) *Subbotina triloculinoides* (364-M0077A-38R-2 60-61 cm); (h) *Eoglobigerina edita* (364-M077A-38R-2 60-61 cm); (i) *Globanomalina compressa* (364-M0077A-37R-1 116-117 cm);

(j) *Praemurica uncinata* (364-M077A-37R-1 96-97 cm); (k) *Praemurica inconstans* (364-M0077A-37R-2 37-38 cm).

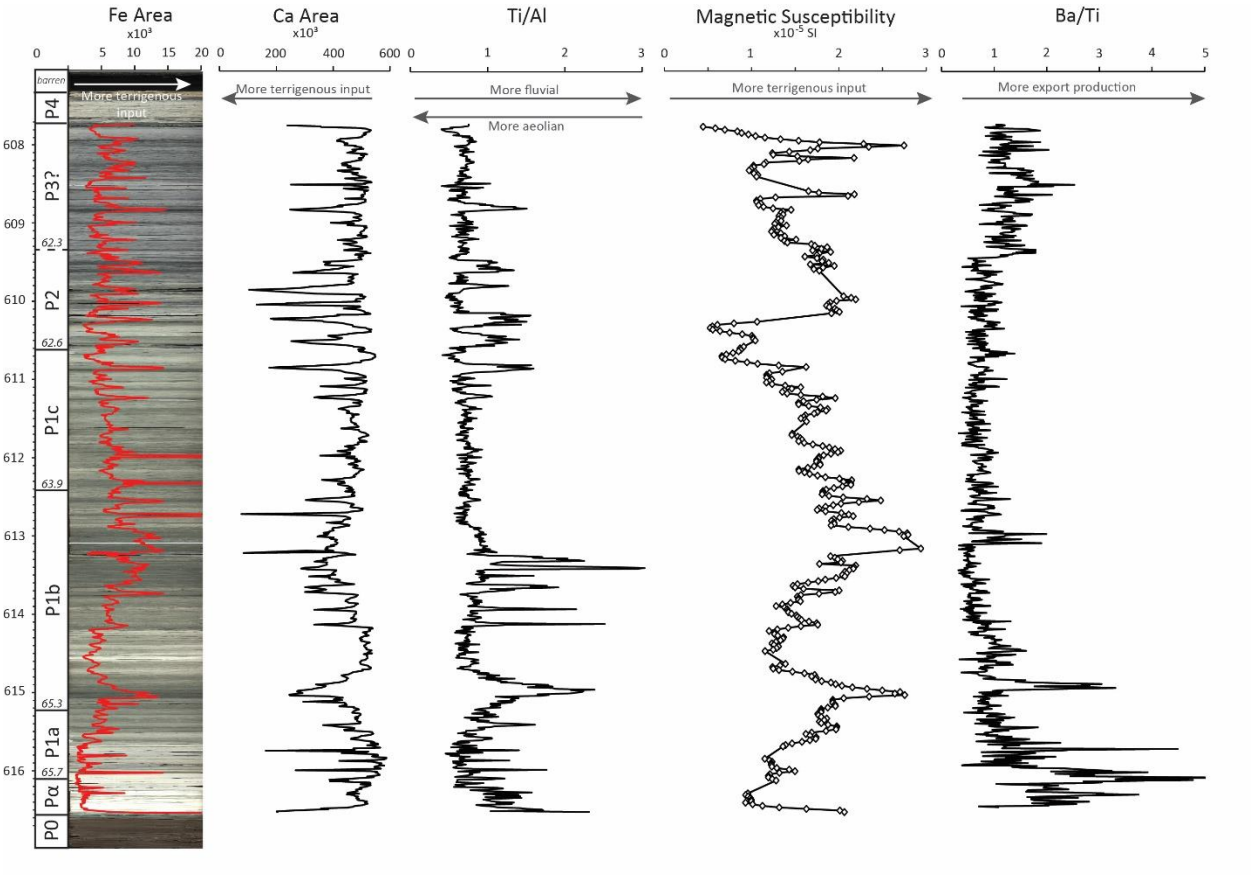

Figure 4. Sedimentological proxies vs. depth. Core linescan composite of the Paleocene interval at Site M0077 is overlaid by XRF Fe counts. Increased Fe, decreased Ca, increased Ti/Al, and higher magnetic susceptibility are all proxies for higher terrigenous flux. Increased Ba/Ti indicated higher local export productivity.

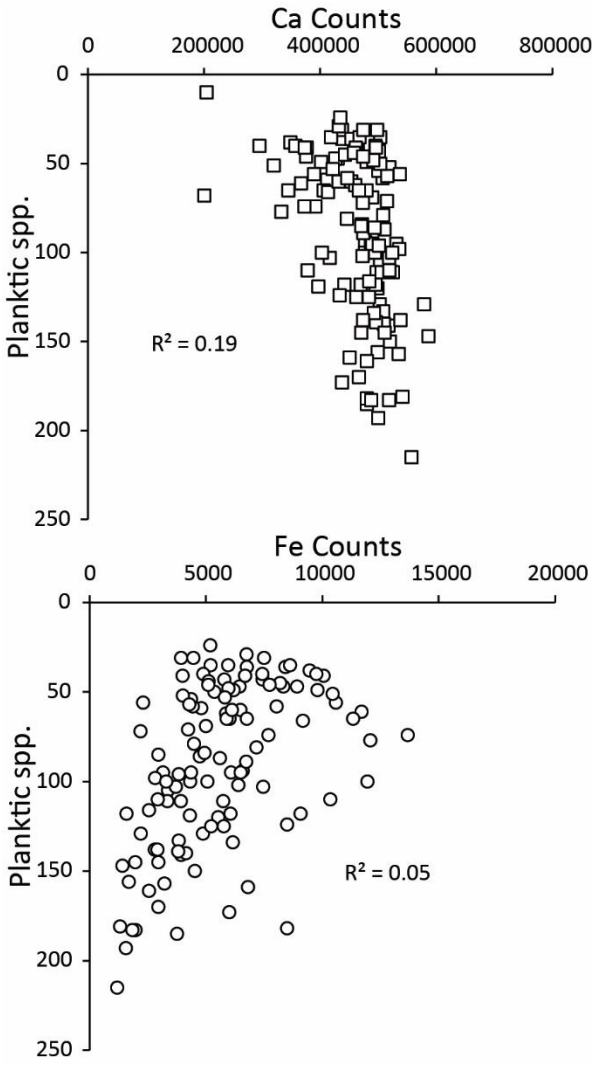

607

608 **Figure 5.** Preservation vs Calcium and Iron XRF counts. Better preservation is toward zero on the y-axis
609 (i.e., fewer unidentifiable foraminifera). Two outliers >80,000 from pyrite-rich samples at the base of the
610 section were removed from the Fe plot. Ca shows a weak negative correlation with good preservation while
611 Fe shows a weak positive correlation with good preservation. This pattern is the opposite of trends caused
612 by dissolution.

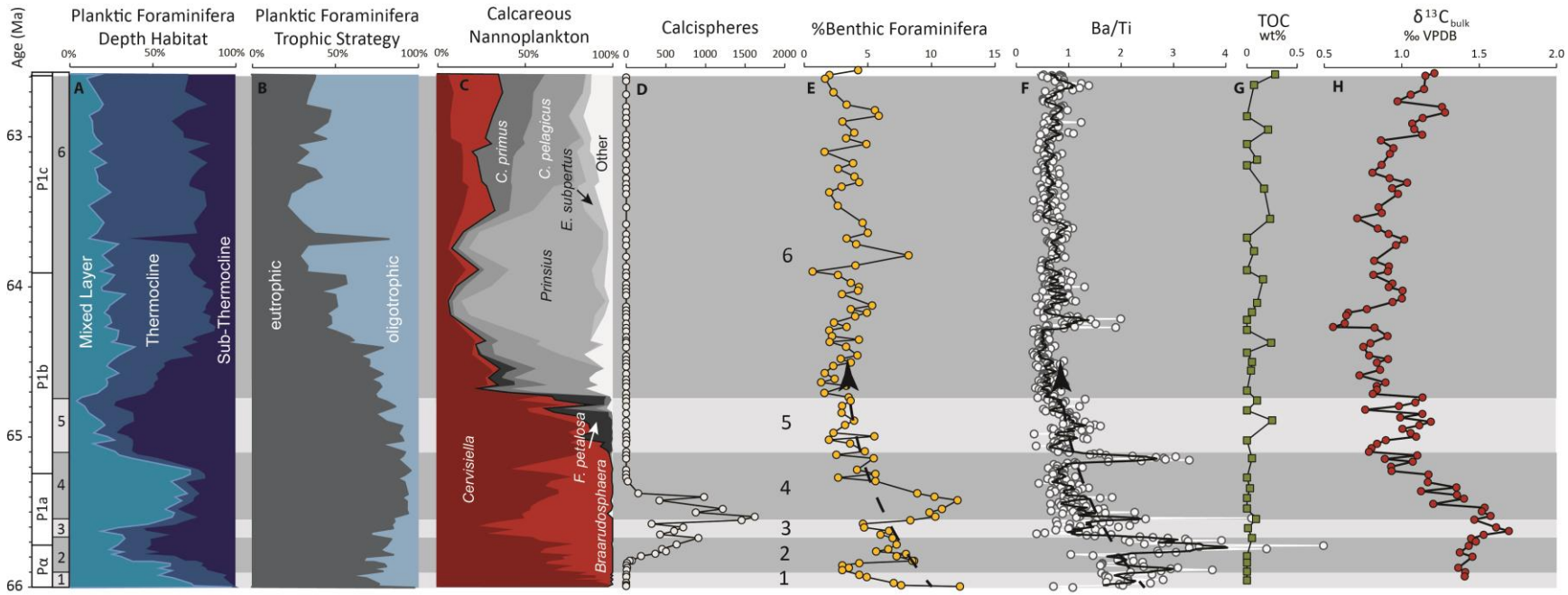

613

614 **Figure 6.** Paleoceanography proxies plotted by age. Planktic foraminifer by depth habitat record the stratification of the upper water column; see
615 Table 2 for species assigned to mixed layer, thermocline, and subthermocline planktic foraminifer groups. Planktic foraminifera by trophic strategy
616 record changes in paleoproductivity in the upper water column, Calcareous nannoplankton diversity shows the relative abundance of all (non-
617 reworked) species of calcareous nannoplankton present; red taxa are the so called "disaster" opportunists, grey are incoming Paleocene taxa.
618 Calcispheres shows the abundance of calcispheres >45 μm. %Benthics is the percentage of benthic foraminifera relative to all foraminifera, and is
619 interpreted to correspond primarily to abundance and quality of nutrient flux to the seafloor. Ba/Ti records paleoproductivity, with high ratios
620 indicating high productivity. TOC (total organic carbon) corresponds to changes in preservation potential of organic carbon at the seafloor. Numbered
621 gray bars represent discrete intervals discussed in Section 4 of the text.

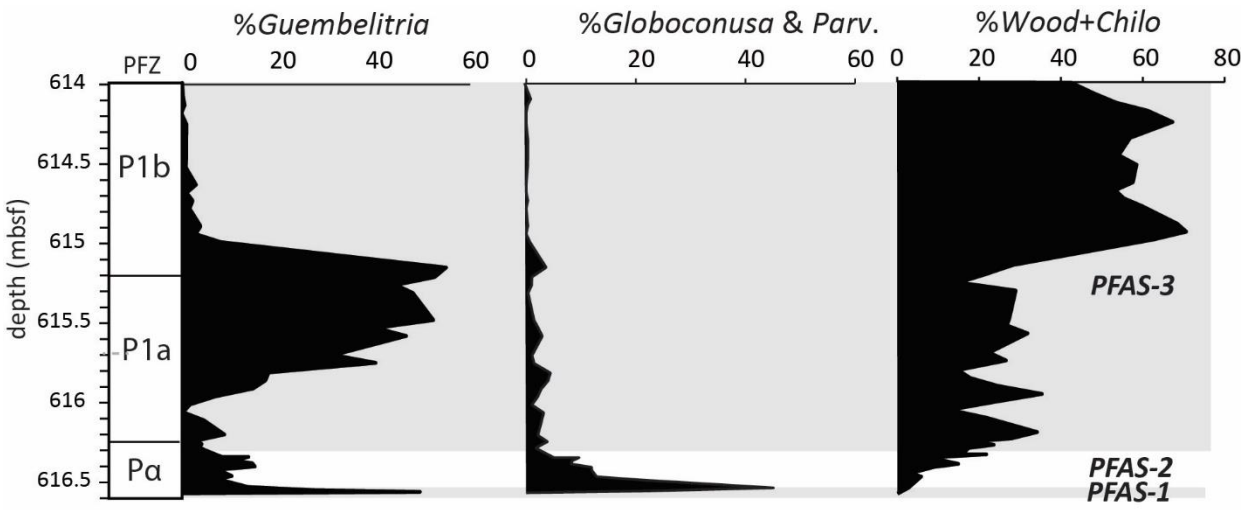

Figure 7. Quantitative stratigraphic distribution of early Danian planktic foraminiferal groups at Site M0077 and Planktic Foraminiferal Acme Stages (PFAS) 1-3: PFAS-1 is the predominance of *Guembelitria*, PFAS-2 is the predominance of *Parvularugoglobigerina* and *Globoconusa* (or *Palaeoglobigerina* according to Arenillas and Arz, 2017), and PFAS-3 is the predominance of *Woodringina* and *Chiloguembelina*. A second acme of *Guembelitria* (or *Chiloguembelitria* according to Arenillas and Arz, 2017) occurs within this stage across the Tethys, as is also evident at Site M0077.

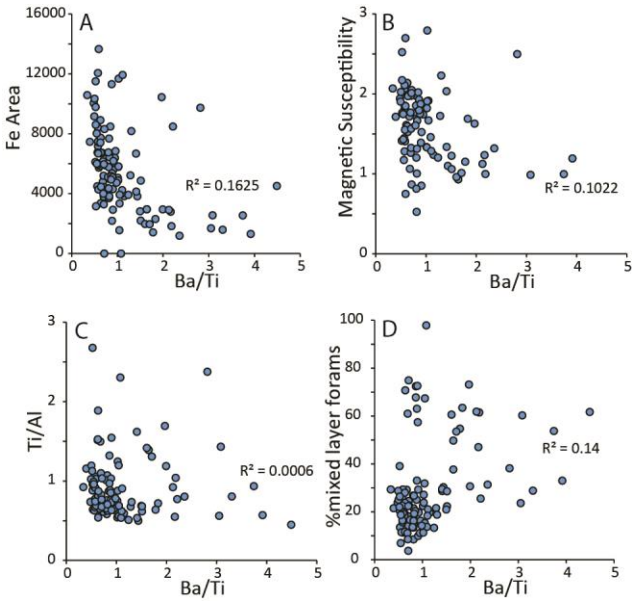

637

638 **Figure 8.** Cross plots of Ba/Ti ratios (i.e., export productivity) with proxies for stratification and terrigenous
639 flux: A) XRF Fe counts, a proxy for sedimentary dilution by terrigenous sediments, B) magnetic
640 susceptibility, a proxy for the influx of terrigenous material, C) Ti/Al, a proxy for the relative abundance
641 of riverine (Ti) vs. aeolian (Al) flux, D) the percent abundance of mixed layer foraminifera vs. total
642 foraminifera, a proxy for the vertical stratification of the upper water column. R^2 values (and your eyeballs,
643 probably) indicate that all 4 are uncorrelated and thus changes in export productivity were not related to
644 terrigenous flux of water column stratification.

645

646

647

648

649

650

651

652 **REFERENCES**

653 Alegret, L., Molina, E., & Thomas, E. (2001). Benthic foraminifera at the Cretaceous-Tertiary boundary
654 around the Gulf of Mexico. *Geology*, 29, 891-894.

655 Alegret, L., & Thomas, E. (2005). Cretaceous/Paleogene boundary bathyal paleo-environments in the
656 central North Pacific (DSDP Site 465), the Northwestern Atlantic (ODP Site 1049), the Gulf of
657 Mexico and the Tethys: The benthic foraminiferal record. *Palaeogeography, Palaeoclimatology,*
658 *Palaeoecology*, 224, 53-82.

659 Alegret, L., Arenillas, I., Arz, J. A., & Molina, E. (2004). Foraminiferal event-stratigraphy across the
660 Cretaceous/Paleogene boundary. *Neues Jahrbuch für Geologie und Paläontologie - Abhandlungen*,
661 234, 25-50.

662 Alegret, L., E. Thomas, & K.C. Lohmann (2012), End-Cretaceous marine mass extinction not caused by
663 productivity collapse, Proceedings of the National Academy of Sciences, 109(3), 728-732.

664 Alvarez, L.W., Alvarez, W., Asaro, F., & Michel, H.V., 1980. Extraterrestrial cause of the Cretaceous–
665 Tertiary extinction. Science 208, 1095–1108.

666 Arenillas, I., Arz, J. A., Molina, E., & Dupuis, C. (2000). An independent test of planktic foraminiferal
667 turnover across the Cretaceous/Paleogene (K/P) boundary at El Kef, Tunisia; catastrophic mass
668 extinction and possible survivorship. *Micropaleontology*, 46, 31-49.

669 Arenillas, I., Arz, J.A., Grajales-Nishimura, J.M., Murillo-Muñetón, G., Alvarez, W., Camargo-Zanoguera,
670 A., Molina, E., Rosales-Domínguez, C. (2006). Chicxulub impact event is Cretaceous/Paleogene
671 boundary in age: new micropaleontological evidence. *Earth and Planetary Science Letters*, 249,
672 241-257.

673 Arenillas, I., Arz, J.A., Grajales-Nishimura, J.M., Rojas-Consuegra, R. (2016). The Chicxulub impact is
674 synchronous with the planktonic foraminifera mass extinction at the Cretaceous/Paleogene
675 boundary: new evidence from the Moncada section, Cuba. *Geologica Acta*, 14(1), 35-51.

676 Arenillas, I., Arz, J.A. (2017). Benthic origin and earliest evolution of the first planktonic foraminifera after
677 the Cretaceous/Paleogene boundary mass extinction. *Historical Biology*, 29, 17-24.

678 Artemieva N. et al., 2017, Quantifying the Release of Climate-Active Gases by Large Meteorite Impacts
679 With a Case Study of Chicxulub, *Geophysical Research Letters*, ISSN: 0094-8276

680 Artemieva, N., & Morgan, J. (2020). Global K-Pg layer deposited from a dust cloud. *Geophysical Research*
681 *Letters*, *47*(6), e2019GL086562.

682 Aze, T., Ezard. T.H.G., Purvis, A., Coxall, H.K., Stewart, D.R.M., Wade, B.S., & Pearson, P.N. (2011), A
683 phylogeny of Cenozoic macroperforate planktonic foraminifera from fossil data, Biological
684 Reviews, 86, 900-927.

685 Bains, S., Norris, R.D., Corfield, R.M., & Faul, K.L. (2000). Termination of global warmth at the
686 Palaeocene/Eocene boundary through productivity feedback. *Nature*, 407, 171.

687 Bardeen, C. G., Garcia, R. R., Toon, O. B., & Conley, A. J. (2017). On transient climate change at the
688 Cretaceous− Paleogene boundary due to atmospheric soot injections. *Proceedings of the National*
689 *Academy of Sciences*, *114*(36), E7415-E7424.

690 Barnet, J.S., Littler, K., Westerhold, T., Kroon, D., Leng, M.J., Bailey, I., Röhl, U., & Zachos, J. C.
691 (2019). A high-Fidelity benthic stable isotope record of late Cretaceous–early Eocene climate
692 change and carbon-cycling. *Paleoceanography and Paleoclimatology*, *34*(4), 672-691.

693 Berggren, W. A., & Pearson, P. N. (2005). A revised tropical to subtropical Paleogene planktonic
694 foraminiferal zonation. *The Journal of Foraminiferal Research*, 35, 279-298.

695 Birch, H. S., Coxall, H. K., & Pearson, P. N. (2012). Evolutionary ecology of Early Paleocene planktonic
696 foraminifera: size, depth habitat and symbiosis. *Paleobiology*, *38*(3), 374-390.

697 Birch, H.S., Coxall, H.K., Pearson, P.N., Kroon, D., & Schmidt, D.N. (2016). Partial collapse of the
698 marine carbon pump after the Cretaceous-Paleogene boundary. *Geology*, 44, 287-290.

699 Boersma, A., & Silva, I.P. (1989). Atlantic Paleogene biserial heterohelicid foraminifera and oxygen
700 minima. *Paleoceanography*, 4, 271-286.

701 Bown, P. (1998). *Calcareous nannofossil biostratigraphy* (pp. 1-315). Chapman and Hall; Kluwer
702 Academic.

703 Boyd, P., & Newton, P. (1995). Evidence of the potential influence of planktonic community structure on
704 the interannual variability of particulate organic carbon flux. *Deep Sea Research Part I:*
705 *Oceanographic Research Papers*, *42*(5), 619-639.

706 Boyd, P.W., & Newton, P.P. (1999). Does planktonic community structure determine downward particulate
707 organic carbon flux in different oceanic provinces?. *Deep Sea Research Part I: Oceanographic*
708 *Research Papers*, *46*(1), 63-91.

709 Boyd, P.W., & Trull, T.W. (2007). Understanding the export of biogenic particles in oceanic waters: is
710 there consensus? *Progress in Oceanography*, *72*(4), 276-312.

711 Boyd, P.W. (2015) Toward quantifying the response of the oceans' biological pump to climate change.
712 *Frontiers of Marine Science* 2, doi: 10.3389/fmars.2015.00077

713 Bralower, T.J., Silva, I.P. & Malone, M.J., 2002. New evidence for abrupt climate change in the Cretaceous
714 and Paleogene: An Ocean Drilling Program expedition to Shatsky Rise, northwest Pacific. *GSA*
715 *TODAY*, *12*, pp.4-10.

716 Bralower, T.J., Cosmidis, J., Heaney, P.J., Kump, L.R., Morgan, J.V., Harper, D.T., Lyons, S.L., Freeman,
717 K.H., Grice, K., Wendler, J., Zachos, J.C., Artimieva, N., Chen, S.A., Gulick, S.P.S., House, C.H.,

718 Jones, H.J., Lowery, C.M., Nims, C., Schaefer, B., Thomas, E., and Vajda, V. (*in revision*) Origin
719 of a global carbonate layer deposited in the aftermath of the Cretaceous-Paleogene boundary
720 impact. *Earth and Planetary Science Letters*.

721 Brugger, J., Feulner, G., & Petri, S. (2017). Baby, it's cold outside: Climate model simulations of the
722 effects of the asteroid impact at the end of the Cretaceous. *Geophysical Research Letters*, 44,
723 419-427.

724 Buesseler, K.O. (1998). The decoupling of production and particulate export in the surface ocean. *Global*
725 *Biogeochemical Cycles*, *12*(2), 297-310.

726 Coccioni, R., Frontalini, F., Bancalà, G., Fornaciari, E., Jovane, L., & Sprovieri, M. (2010). The Dan-C2
727 hyperthermal event at Gubbio (Italy): Global implications, environmental effects, and
728 cause(s). *Earth and Planetary Science Letters*, 297, 298-305.

729 Collins, G.S., Patel, N., Rae, A.S., Davies, T.M., Morgan, J.V. Gulick, S.P.S. and Expedition 364
730 Scientists (2017). Numerical simulations of Chicxulub crater formation by oblique impact. *Lunar*
731 *and Planetary Science Conference XLVII*, abstract #1832.

732 Coxall, H.K., S. D'Hondt, & J.C. Zachos (2006), Pelagic evolution and environmental recovery after the
733 Cretaceous-Paleogene mass extinction, Geology, 34(4), 297-300.

734 Culver, S.J. (1988), New foraminiferal depth zonation of the northwestern Gulf of Mexico, *Palaios*, 3,
735 69–85.

736 Culver, S. J. (2003). Benthic foraminifera across the Cretaceous–Tertiary (K–T) boundary: a
737 review. *Marine Micropaleontology*, *47*(3-4), 177-226.

738 D'Hondt, S., & Keller, G. (1991). Some patterns of planktic foraminiferal assemblage turnover at the
739 Cretaceous-Tertiary boundary. *Marine Micropaleontology*, 17, 77-118.

740 D'Hondt, S., & Zachos, J.C. (1993). On stable isotopic variation and earliest Paleocene planktonic
741 foraminifera. *Paleoceanography*, 8, 527-547.

742 D'Hondt, S., King, J., & Gibson, C. (1996). Oscillatory marine response to the Cretaceous-Tertiary
743 impact. *Geology*, 24, 611-614.

744 D'Hondt, S., Donaghay, P., Zachos, J.C., Luttenberg, D., & Lindinger, M. (1998). Organic carbon fluxes
745 and ecological recovery from the Cretaceous-Tertiary mass extinction. *Science*, 282, 276-279.

746 D'Hondt, S., & Zachos, J.C. (1998). Cretaceous foraminifera and the evolutionary history of planktic
747 photosymbiosis. *Paleobiology*, 24, 512-523.

748 D'Onofrio, R., Luciani, V., Fornaciari, E., Giusberti, L., Boscolo Galazzo, F., Dallanave, E., ... & Telch,
749 S. (2016). Environmental perturbations at the early Eocene ETM2, H2, and I1 events as inferred
750 by Tethyan calcareous plankton (Terche section, northeastern Italy). *Paleoceanography*, *31*(9),
751 1225-1247.

752 De La Rocha, C.L. & Passow, U. (2007). Factors influencing the sinking of POC and the efficiency of the
753 biological carbon pump. *Deep Sea Research Part II: Topical Studies in Oceanography*, *54*(5-7),
754 639-658.

755 Dymond, J., Suess, E., & Lyle, M. (1992). Barium in deep-sea sediment: A geochemical proxy for
756 paleoproductivity, *Paleoceanography*, 7, 163-181. doi:10.1029/92PA00181

757 Eagle, M., Paytan, A., Arrigo, K.R., van Dijken, G., & Murray, R.W. (2003). A comparison between excess
758 barium and barite as indicators of carbon export, *Paleoceanography*, 18, 1021.
759 doi:10.1029/2002PA000793

760 Edgar, K.M., Wilson, P.A., Sexton, P.F., & Suganuma, Y., (2007) No extreme glaciation during the main
761 Eocene calcite compensation depth shift, *Nature*, 448, 908-911.

762 Esmeray-Senlet, S., Wright, J.D., Olsson, R.K., Miller, K.G., Browning, J.V., & Quan, T.M. (2015).
763 Evidence for reduced export productivity following the Cretaceous/Paleogene mass extinction,
764 Paleoceanography, 30, doi:10.1002/2014PA002724.

765 Fraass, A.J., Kelly, D.C., & Peters, S.E. (2015), Macroevolutionary history of the planktic
766 foraminifera *Annual Reviews of Earth and Planetary Science*, 43, 139-166.

767 Francois, R., Honjo, S., Manganini, S.J., & Ravizza, G.E. (1995). Biogenic barium fluxes to the deep sea:
768 Implications for paleoproductivity reconstruction, *Global Biogeochemical Cycles*, 9, 289-303.
769 doi:10.1029/95GB00021.

770 Galloway, W.E., Ganey-Curry, P.E., Li, X., & Buffler, R.T. (2000), Cenozoic depositional history of the
771 Gulf of Mexico basin, *AAPG Bulletin*, 84, 1743-1774.

772 Gertsch, B., Keller, G., Adatte, T., Garg, R., Prasad, V., Berner, Z., & Fleitmann, D. Environmental effects
773 of Deccan volcanism across the Cretaceous–Tertiary transition in Meghalaya, India, *Earth and*
774 *Planetary Science Letters* 310 272-285 (2011).

775 Gibbs, S.J., Bralower, T.J., Bown, P.R., Zachos, J.C., & Bybell, L.M. (2006). Shelf and open-ocean
776 calcareous phytoplankton assemblages across the Paleocene-Eocene Thermal Maximum:
777 Implications for global productivity gradients. *Geology*, 34, 233-236.

778 Gooday, A.J., (2003), Benthic Foraminifera (Protista) as tools in deep-water palaeoceanography:
779 environmental influences on faunal characteristics, *Advances in Marine Biology*, 46, 1–90.

780 Govin, A., Holzwarth, U., Heslop, D., Ford Keeling, L., Zabel, M., Mulitza, S., Collins, J.A., & Chiessi,
781 C.M. (2012). Distribution of major elements in Atlantic surface sediments (36 N–49 S): Imprint
782 of terrigenous input and continental weathering. *Geochemistry, Geophysics, Geosystems*, 13.

783 Gradstein, F.M., Ogg, J.G., Schmitz, M., & Ogg, G., Eds. (2012), *The Geologic Times Scale 2012*.
784 Elsevier B.V., Amsterdam, Netherlands.

785 Griffith, E.M., & Paytan, A. (2012). Barite in the ocean–occurrence, geochemistry and
786 palaeoceanographic applications. *Sedimentology*, 59, 1817-1835.

787 Gulick, S.P., Barton, P.J., Christeson, G.L., Morgan, J.V., McDonald, M., Mendoza-Cervantes, K.,
788 Pearson, Z.F., Surendra, A., Urrutia-Fucugauchi, J., Vermeesch, P.M., & Warner, M.R. (2008).
789 Importance of pre-impact crustal structure for the asymmetry of the Chicxulub impact
790 crater. *Nature Geoscience*, 1, 131.

791 Gulick, S., Morgan, J., Mellett, C.L., Green, S.L., Bralower, T., Chenot, E., Christeson, G., Claeys, P.,
792 Cockell, C., Coolen, M.J.L., Ferrière, L., Gebhardt, C., Goto, K., Jones, H., Kring, D., Lofi, J.,
793 Lowery, C., Ocampo-Torres, R., Perez-Cruz, L., Pickersgill, A.E., Poelchau, M., Rae, A.,
794 Rasmussen, C., Rebolledo-Vieyra, M., Riller, U., Sato, H., Smit, J., Tikoo, S., Tomioka, N.,
795 Urrutia- Fucugauchi, J., Whalen, M., Wittmann, A., Yamaguchi, K., Xiao, L., & Zylberman, W.,
796 2017. Site M0077: Post-Impact Sedimentary Rocks. *In* Morgan, J., Gulick, S., Mellett, C.L.,
797 Green, S.L., and the Expedition 364 Scientists, *Chicxulub: Drilling the K-Pg Impact*
798 *Crater.* Proceedings of the International Ocean Discovery Program, 364: College Station, TX
799 (International Ocean Discovery Program). https://doi.org/10.14379/iodp.proc.364.105.2017

800 Gulick, S.P.S., Bralower, T.J., Ormö, J., Hall, B., Grice, K., Schaefer, B., Lyons, S., Freeman, K.H.,
801 Morgan, J.V., Artemieva, N., Kaskes, P., de Graff, S.J., Whalen, M.T., Collins, S.M., Verhagen,
802 C., Christeson, G.L., Claeys, P., Coolen, M.J., Goderis, S., Goto, K., Grieve, R., McCall, N.,
803 Osinksi, G.R., Rae, A., Riller, U., Smit, J., Vajda, V., Wittman, A., and Expedition 364 Scientists,
804 (2019) The First Day of the Cenozoic. *Proceedings of the National Academy of Sciences*, 116,
805 19342-19351.

806 Hemleben, C., Spindler, M., & Anderson, O. R. (1989). *Modern planktonic foraminifera*. Springer
807 Science & Business Media.

Hemleben, C., Mühlen, D., Olsson, R.K., & Berggren, W.A. (1991). Surface texture and the first occurrence of spines in planktonic foraminifera from the early Tertiary. *Geologisches Jahrbuch*, 128, 117-146.

Henehan, M. J., Ridgwell, A., Thomas, E., Zhang, S., Alegret, L., Schmidt, D. N., Rae, J.W.B., Witts, J.D., Landman, N.H., Greene, S.H., Huber, B.T., Super, J.R., Planavsky, N.J., & Hull, P.M. (2019). Rapid ocean acidification and protracted Earth system recovery followed the end-Cretaceous Chicxulub impact. *Proceedings of the National Academy of Sciences*, *116*(45), 22500-22504.

Henson, S.A., Sanders, R., & Madsen, E. (2012), Global patterns in efficiency of particulate organic carbon export and transfer to the deep ocean, *Global Biogeochem. Cycles*, 26, GB1028, doi:10.1029/2011GB004099.

Hildebrand, A.R., Penfield, G.T., Kring, D.A., Pilkington, M., Camargo, A.Z., Jacobsen, S.B., & Boynton, W.V. (1991). Chicxulub Crater: a possible Cretaceous/Tertiary boundary impact crater on the Yucatán Peninsula, Mexico. Geology 19, 867–871.

Hsü, K.J., & McKenzie, J.A. (1985). A "Strangelove" ocean in the earliest Tertiary. *The Carbon Cycle and Atmospheric CO: Natural Variations Archean to Present*, 487-492.

Hull, P.M., & R.D. Norris (2011), Diverse patterns of ocean export productivity change across the Cretaceous-Paleogene boundary: New insights from biogenic barium, Paleoceanography, 26(3).

Hull, P. M., Norris, R. D., Bralower, T. J., & Schueth, J. D. (2011). A role for chance in marine recovery from the end-Cretaceous extinction. *Nature Geoscience*, 4, 856-860.

Jablonski, D. (1995) in *Extinction Rates* (eds. Lawton, J. H. & May, R. M.) 25–44 Oxford Univ. Press, Oxford.

Jehle, S., Bornemann, A., Deprez, A., & Speijer, R.P. (2015). The impact of the latest Danian event on planktic foraminiferal faunas at ODP site 1210 (Shatsky rise, Pacific Ocean). *PloS one*, 10, e0141644.

Jiang, S., T.J. Bralower, M.E. Patzkowsky, L.R. Kump, &J.D. Schueth (2010), Geographic controls on nannoplankton extinction across the Cretaceous/Palaeogene boundary, Nature Geoscience, 3(4), 280.

Jones, H., Lowery, C.M., and Bralower, T. (2019). Delayed calcareous nannoplankton boom-bust successions in the earliest Paleocene Chicxulub (Mexico) impact Crater. *Geology*, 47 753-756 https://doi.org/10.1130/G46143.1

Jorissen, F.J., H.C. de Stigter, & J.G.V. Widmark, (1995), A conceptual model explaining benthic foraminiferal microhabitats, *Marine Micropaleontology*, 26, 3–15.

Keller, G. (1989). Extended Cretaceous/Tertiary boundary extinctions and delayed population change in planktonic foraminifera from Brazos River, Texas. *Paleoceanography and Paleoclimatology*, 4, 287-332.

Knoll, A.H. & Follows, M.J. (2016) A bottom-up perspective on ecosystem change in Mesozoic oceans, *Proceedings of the Royal Society B* 283 2016755.

Kring, D. A. (2007). The Chicxulub impact event and its environmental consequences at the Cretaceous–Tertiary boundary: *Palaeogeography, Palaeoclimatology, Palaeoecology*, 255, 4-21.

Lam, P.J., Doney, S.C., & Bishop, J.K.B. (2011). The dynamic ocean biological pump: Insights from a global compilation of particulate organic carbon, CaCO3 and opal concentration profiles from the mesopelagic. *Global Biogeochemical Cycles* 27, GB3009.

Leckie, R.M., Bralower, T.J., & Cashman, R. (2002). Oceanic anoxic events and plankton evolution: Biotic response to tectonic forcing during the mid-Cretaceous. *Paleoceanography*, 17, 13-1.

Leckie, R.M., & H.C. Olson, (2003), Foraminifera as proxies for sea-level change on siliciclastic margins, *in*: Olson, H.C., and R.M. Leckie, eds., *Micropaleontologic proxies for sea-level change and stratigraphic discontinuities, SEPM Special Publication No.* 75, 5–19.

Legendre, L., & Michaud, J. (1998). Flux of biogenic carbon in oceans: size-dependent regulation by pelagic food webs. *Marine Ecology Progress Series, 164,* 1-11.

Legendre, L. & Rivkin, R.B. (2002). Fluxes of carbon in the upper ocean: regulation by food-web control nodes. *Marine Ecology Progress Series*, 242, 95-109.

Lirer, F. (2000). A new technique for retrieving calcareous microfossils from lithified lime deposits. *Micropaleontology* 46, 365-369.

Liu, C., & Olsson, R.K. (1992). Evolutionary radiation of microperforate planktonic foraminifera following the K/T mass extinction event. *The Journal of Foraminiferal Research*, 22, 328-346.

Liu, Q., Roberts, A. P., Larrasoana, J. C., Banerjee, S. K., Guyodo, Y., Tauxe, L., & Oldfield, F. (2012). Environmental magnetism: principles and applications. *Reviews of Geophysics*, 50, RG4002, doi:10.1029/2012RG000393.

Lowery, C.M. et al., 2018, Rapid Recovery of Life At Ground Zero of the End Cretaceous Mass Extinction, *Nature* v. 558, p. 288-291, https://doi.org/10.1038/s41586-018-0163-6

Lowery, C.M. & Fraass, A.J. (2019). Explanation for delayed recovery of species diversity following the end Cretaceous mass extinction. *Nature Ecology and Evolution* https://doi.org/10.1038/s41559-019-0835-0

Lowery, C.M., Bralower, T.J., Christeson, G., Gulick, S.P.S., Morgan, J.V., and Expedition 364 Scientists (2019). Ocean Drilling Perspectives on Meteorite Impacts. *Oceanography* 32, 120-134. https://doi.org/10.5670/oceanog.2019.133

Lowery, C. M., Bown, P. R., Fraass, A. J., & Hull, P. M. (2020). Ecological Response of Plankton to Environmental Change: Thresholds for Extinction. *Annual Review of Earth and Planetary Sciences*, 48.

MacLeod, K. G., Quinton, P. C., Sepúlveda, J., & Negra, M. H. (2018). Postimpact earliest Paleogene warming shown by fish debris oxygen isotopes (El Kef, Tunisia). *Science*, 360(6396), 1467-1469.

Miller, K. G., Browning, J. V., Schmelz, W. J., Kopp, R. E., Mountain, G. S., & Wright, J. D. (2020). Cenozoic sea-level and cryospheric evolution from deep-sea geochemical and continental margin records. *Science advances*, *6*(20), eaaz1346.

Morgan, J.V., S.P.S. Gulick, C.L. Mellet, S.L. Green, & Expedition 364 Scientists (2017) *Chicxulub: Drilling the K-Pg Impact Crater, Proceedings of the International Ocean Discovery Program, 364*, International Ocean Discovery Program, College Station, TX, doi: 10.14379/iodp.proc.364.103.2017.

Murray, J.W. (1976), A method of determining proximity of marginal seas to an ocean, *Marine Geology*, 22, 103–119.

Norris, R. D. (1996). Symbiosis as an evolutionary innovation in the radiation of Paleocene planktic foraminifera. *Paleobiology*, 22, 461-480.

Okada, H., and Bukry, D. (1980). Supplementary modification and introduction of code numbers to the low-latitude coccolith biostratigraphic zonation (Bukry, 1973; 1975). *Marine Micropaleontology*, 5, 321-325.

Olsson, R. K., Berggren, W. A., Hemleben, C. I., & Huber, B. T. (1999). Atlas of Paleocene planktonic foraminifera. *Smithsonian Contributions to Paleobiology* 85.

Paytan, A., Kastner, M., and Chavez, F.P. (1996). Glacial to interglacial fluctuations in productivity in the equatorial Pacific as indicated by marine barite. *Science*, 274, 1355-1357.

898 Paytan, A., and Griffith, E.M. (2007). Marine barite: Recorder of variations in ocean export productivity,
899 in *Encyclopedia of Paleoclimate and Ancient Environments*, Gornitz, V., Ed., p. 643-651, Springer,
900 New York.

901 Pearson, P.N., Olsson, R.K., Huber, B.T., Hemleben, C., and Berggren, W. A. (2006). Atlas of Eocene
902 Planktonic Foraminifera, Cushman Foundation for Foraminiferal Research Special Publications,
903 vol. 41. Washington, DC, 513.

904 Pedersen, T. F., & Calvert, S. E. (1990). Anoxia vs. productivity: what controls the formation of organic-
905 carbon-rich sediments and sedimentary Rocks?. *AAPG Bulletin*, *74*(4), 454-466.

906 Perch-Nielsen, K. (1985). Cenozoic calcareous nannofossils. *In* Bolli, H.M., Saunders, J.B., and Perch-
907 Nielsen, K. (Eds.) *Plankton stratigraphy*, Cambridge: Cambridge University Press. 427-554.

908 Pope, K. O., Baines, K. H., Ocampo, A. C., & Ivanov, B. A. (1994). Impact winter and the
909 Cretaceous/Tertiary extinctions: Results of a Chicxulub asteroid impact model. *Earth and*
910 *Planetary Science Letters*, *128*(3-4), 719-725.

911 Punekar, J., Mateo, P., & Keller, G. (2014a) Effects of Deccan volcanism on paleoenvironment and planktic
912 foraminifera: A global survey, *Geological Society of America Special Papers*, 505, 91-116.

913 Punekar, J., Keller, G., Khozyem, H., Hamming, C., Adatte, T., Tantawy, A.A., & Spangenberg, J.E.
914 (2014b) Late Maastrichtian–early Danian high-stress environments and delayed recovery linked to
915 Deccan volcanism, *Cretaceous Research*, 49, 63-82.

916 Quillévéré, F., Norris, R.D., Kroon, D., and Wilson, P.A. (2008). Transient ocean warming and shifts in
917 carbon reservoirs during the early Danian. *Earth and Planetary Science Letters*, 265, 600-615.

918 Renne, P.R., Sprain, C.J., Richards, M.A., Self, S., Vanderkluysen, L., & Pande, K. (2015) State shift in
919 Deccan volcanism at the Cretaceous-Paleogene boundary, possibly induced by impact, *Science*,
920 350**,** 76-78.

Rodriguez-Tovar, F. J., Lowery, C. M., Bralower, T. J., Gulick, S. P. S., & Jones, H. L. (*in revision*) Rapid microbenthic diversification and stabilization after the end-Cretaceous mass extinction event. *Geology*.

Rothwell R., & Croudace I. (2015). Twenty Years of XRF Core Scanning Marine Sediments: What Do Geochemical Proxies Tell Us?. In: Croudace I., Rothwell R. (eds) *Micro-XRF Studies of Sediment Cores. Developments in Paleoenvironmental Research*, 17. Springer, Dordrecht

Schaefer, B. Grice, K., Coolen, M.J.L., Summons, R.E., Cui, X., Bauersachs, T., Schwark, L., Böttcher, M.E., Bralower, T.J., Lyons, S.L., Freeman, K.H., Cockell, C.S., Gulick, S.P.S., Morgan, J.V., Whalen, M.T., Lowery, C.M., and Vajda, V. (2020) Microbial life in the nascent Chicxulub crater. *Geology*. 48, https://doi.org/10.1130/G46799.1

Schoene, B., Eddy, M. P., Samperton, K. M., Keller, C. B., Keller, G., Adatte, T., & Khadri, S. F. (2019). U-Pb constraints on pulsed eruption of the Deccan Traps across the end-Cretaceous mass extinction. *Science*, *363*(6429), 862-866.

Schueth, J. D., T. J. Bralower, S. Jiang, and M. E. Patzkowsky (2015), The role of regional survivor incumbency in the evolutionary recovery of calcareous nannoplankton from the Cretaceous/Paleogene (K/Pg) mass extinction, Paleobiology, 41(4), 661-679.

Schulte, P. and 40 others, (2010), The Chicxulub asteroid impact and mass extinction at the Cretaceous-Paleogene boundary, Science, 327, 1214-1218.

Sepúlveda, J., Wendler, J.E., Summons, R.E., & Hinrichs, K.U. (2009). Rapid resurgence of marine productivity after the Cretaceous-Paleogene mass extinction. *Science*, 326, 129-132.

Sigman, D. M. & Hain, M. P. (2012) The Biological Productivity of the Ocean. *Nature Education Knowledge* 3, p. 21

Smit, J. and J. Hertogen (1980). An extraterrestrial event at the Cretaceous-Tertiary boundary, Nature 285: 198-200.

945 Sprain, C. J., Renne, P. R., Vanderkluysen, L., Pande, K., Self, S., & Mittal, T. (2019). The eruptive tempo
946 of Deccan volcanism in relation to the Cretaceous-Paleogene boundary. *Science*, *363*(6429), 866-
947 870.

948 Tabor, C.R., Bardeen, C.G., Otto-Bliesner, B.L., Garcia, R.R., & Toon, O.B. (2020). Causes and Climatic
949 Consequences of the Impact Winter at the Cretaceous-Paleogene Boundary. *Geophysical Research*
950 *Letters*, 47, e60121.

951 Thunell, R.C. (1976). Optimum indices of calcium carbonate dissolution, in deep-sea sediments. *Geology*,
952 4, 525-528.

953 Troelsen, J.C. (1957). Some planktonic foraminifera of the type Danian and their stratigraphic
954 importance. *US National Museum Bulletin*, 215, 125-131.

955 Tschudy, R. H., Pillmore, C. L., Orth, C. J., Gilmore, J. S., & Knight, J. D. (1984). Disruption of the
956 terrestrial plant ecosystem at the Cretaceous-Tertiary boundary, Western
957 Interior. *Science*, *225*(4666), 1030-1032.

958 Tsikos, H., Jenkyns, H.C., Walsworth-Bell, B., Petrizzo, M.R., Forster, A., Kolonic, S., Erba, E., Silva, I.P.,
959 Baas, M., Wagner, T., & Damsté, J.S. (2004). Carbon-isotope stratigraphy recorded by the
960 Cenomanian–Turonian Oceanic Anoxic Event: correlation and implications based on three key
961 localities. *Journal of the Geological Society*, *161*(4), 711-719.

962 Vajda, V., Raine, J. I., Hollis, C. J., & Strong, C. P. (2004). Global effects of the Chicxulub impact on
963 terrestrial vegetation—review of the palynological record from New Zealand Cretaceous/Tertiary
964 boundary. In *Cratering in marine environments and on ice* (pp. 57-74). Springer, Berlin,
965 Heidelberg.

966 Van der Zwaan, G.J., Jorissen, F.J. & Stitger, H.C. (1990), The depth dependency of planktonic/benthic
967 foraminiferal ratios: constraints and applications, *Marine Geology*, 95, 1–16.

968 Van Hinsbergen, D.J.J., Kouwenhoven, T.J., & Van der Zwaan, G.J. (2005), Paleobathymetry in the
969 backstripping procedure: correction of oxygenation effects on depth estimates, *Palaeogeography,*
970 *Palaeoclimatology, Palaeoceology*, 21, 245–265.

971 Vellekoop, J., Sluijs, A., Smit, J., Schouten, S., Weijers, J.W.H., Sinninghe Damsté, J.S., & Brinkhuis, H.,
972 (2014). Rapid short-term cooling following the Chicxulub impact at the Cretaceous–Paleogene
973 boundary. *PNAS*, 111, 7537-7541.

974 Vellekoop, J., Woelders, L., Açikalin, S., Smit, J., Van De Schootbrugge, B., Yilmaz, I.O., Brinkhuis, H.,
975 & Speijer, R. (2017). Ecological response to collapse of the biological pump following the mass
976 extinction at the Cretaceous-Paleogene boundary. *Biogeosciences*, 14, 885-900.

977 Wade, B.S., Pearson, P.N., Berggren, W.A., & Pälike, H. (2011). Review and revision of Cenozoic tropical
978 planktonic foraminiferal biostratigraphy and calibration to the geomagnetic polarity and
979 astronomical time scale. *Earth-Science Reviews*, 104, 111-142.

980 Wolbach, W. S., Lewis, R. S., & Anders, E. (1985). Cretaceous extinctions: evidence for wildfires and
981 search for meteoritic material. *Science*, *230*(4722), 167-170.

982 Zachos, J.C., Arthur, M.A., & Dean, W.E. (1989). Geochemical evidence for suppression of pelagic marine
983 productivity at the Cretaceous/Tertiary boundary. *Nature*, 337, 61-64.

984 Zhang, C., Dang, H., Azam, F., Benner, R., Legendre, L., Passow, U., Polimene, L., Robinson, C., Suttle,
985 C.A., & Jiao, N. (2018). Evolving paradigms in biological carbon cycling in the ocean. *National*
986 *Science Review* 5, 481-499.

987 Ziegler M., Lourens L. J., Tuenter E., & Reichart G. J. (2009). Anomalously high Arabian Sea productivity
988 conditions during MIS 13. *Climate of the Past Discussion* 5:1989–2018. (www.clim-past-
989 discuss.net/5/1989/2009/)

990